Guided-Ion Beam and Theoretical Study of the Potential Energy Surface for Activation of Methane by W^{+}†

P. B. Armentrout,* Saeyoung Shin, and Rohana Liyanage‡

Department of Chemistry, University of Utah, Salt Lake City, Utah 84112

Received: May 24, 2005; In Final Form: June 28, 2005

A guided-ion beam tandem mass spectrometer is used to study the reactions, $W^+ + CH_4$ (CD_4) and $[W,C,2H]^+ + H_2$ (D_2), to probe the $[W,C,4H]^+$ potential energy surface. The reaction $W^+ + CH_4$ produces $[W,C,2H]^+$ in the only low-energy process. The analogous reaction in the CD_4 system exhibits a cross section with strong differences at the lowest energies caused by zero-point energy differences, demonstrating that this reaction is slightly exothermic for CH_4 and slightly endothermic for CD_4. The $[W,C,2H]^+$ product ion reacts further at thermal energies with CH_4 to produce $W(CH_2)_x^+$ ($x = 2-4$). At higher energies, the $W^+ + CH_4$ reaction forms WH^+ as the dominant ionic product with smaller amounts of WCH_3^+, WCH^+, and WC^+ also formed. The energy dependent cross sections for endothermic formation of the various products are analyzed and allow the determination of $D_0(W^+-CH_3) \sim 2.31 \pm 0.10$ eV, $D_0(W^+-CH_2) = 4.74 \pm 0.03$ eV, $D_0(W^+-CH) = 6.01 \pm 0.28$ eV, and $D_0(W^+-C) = 4.96 \pm 0.22$ eV. We also examine the reverse reaction, $[W,C,2H]^+ + H_2$ (D_2) → $W^+ + CH_4$ (CH_2D_2). Combining the cross sections for the forward and reverse processes yields an equilibrium constant from which $D_0(W^+-CH_2) = 4.72 \pm 0.04$ eV is derived. Theoretical calculations performed at the B3LYP/HW+/6-311++G(3df,3p) level yield thermochemistry in reasonable agreement with experiment. These calculations help identify the structures and electronic states of the species involved and characterize the potential energy surface for the $[W,C,4H]^+$ system.

Introduction

In the gas phase, third-row transition metal elements are much more reactive with alkanes than first- and second-row metals,[1−7] a result that finds parallels in solution-phase C−H bond activation chemistry.[8] W^+ has been reported as one of the most reactive of these elements. In an ion cyclotron resonance (ICR) mass spectrometry study at thermal energies, Irikura and Beauchamp reported that W^+ reacts rapidly four times with methane by sequential dehydrogenations to form $WC_4H_8^+$.[1] Subsequent reactions occur more slowly, but lead as far as $WC_8H_{16}^+$.[1] Irikura and Beauchamp also found a strong isotope effect,[2] where $^{13}CD_4$ appears to react only with excited W^+. Subsequent reactions of $W^{13}CD_2^+$ are rapid and lead to $W^{13}C_4D_8^+$. Mourgues et al. reported that W^+ reacts rapidly at thermal energies with all hydrocarbons smaller than hexane except acetylene.[3] Simon et al. have studied the $[W,C,2H]^+$ product by photodissociation spectroscopy, obtaining a value of 2.5 ± 0.1 eV to form $WCH^+ + H$.[9] Complementary theoretical results have helped to explain the strong reactivity of W^+.[5,9−12] Irikura and Goddard calculated the low-lying states of WCH_2^+,[10] although the more detailed calculations of Simon et al. demonstrate the existence of two isomers of $[W,C,2H]^+$, a strongly distorted carbene, WCH_2^+, and a hydride carbyne, $HWCH^+$.[9] Goddard and co-workers have reported theoretical values for the bond energies of W^+-H,[11] W^+-CH_2,[10] and an estimate for W^+-CH,[10] whereas Holthausen et al. have examined the thermochemistry of W^+-CH_3.[12]

To better understand this very reactive system and the chemistry of tungsten in general, it would be desirable to obtain thermodynamic data on the products and intermediates. As part of an ongoing project in our laboratory, we have recently extended our studies of the reactions of atomic transition metal ions with small hydrocarbons to third-row metals.[13,14] Extensive work for first- and second-row transition metal ions provides an examination of the electronic requirements for C−H and C−C bond activation at metal centers and the periodic trends in their reactivities.[15−24] Kinetic energy dependent studies have allowed us to obtain metal−hydrogen and metal−carbon bond dissociation energies (BDEs)[25−27] and to probe the potential energy surfaces (PESs) of the reaction.[13,14,28,29] In the present study, we extend this work to examine W^+ and explore the PES for the $[W,C,4H]^+$ system. The reaction of W^+ with methane, as well as its reverse, $[W,C,2H]^+ + H_2$, and their deuterated analogues, are examined over a broad range of energies using a guided-ion beam tandem mass spectrometer. Complementary theoretical work is also performed to examine details of the product ions and PES.

Experimental and Theoretical Section

The experiments are performed using a guided ion beam tandem mass spectrometer equipped with a dc discharge/flow tube ion source, as described in detail elsewhere.[30,31] The ions are formed as described below, extracted from the source, accelerated, and passed through a magnetic sector momentum analyzer for mass analysis. The mass selected ions are decelerated to the desired kinetic energy and focused into an octopole ion guide that radially traps the ions.[32] While in the octopole, the ions pass through a gas cell, which contains the neutral reactant. The product ions and the unreacted parent ions drift out of the gas cell, are extracted from the octopole guide, focused into a quadrupole mass filter, and detected by a secondary

† Part of the special issue "William Hase Festschrift".

‡ Current address: Department of Chemistry and Biochemistry, University of Arkansas.

10.1021/jp052732p CCC: $33.50
Published on Web 08/12/2005

electron scintillation detector. Ion intensities are converted to absolute cross sections as described previously.[33] Uncertainties in the absolute cross sections are estimated at ±20% with relative uncertainties generally good to about ±5%.

To determine the absolute zero and distribution of the ion kinetic energy, the octopole is used as a retarding energy analyzer.[33] The uncertainty in the absolute energy scale is ±0.05 eV (lab) and the full width at half-maximum (fwhm) of the ion energy distributions is about 0.7 eV (lab). Lab energies are converted into center-of-mass energies using $E(\mathrm{CM}) = E(\mathrm{lab})M/(m + M)$ where m and M are the masses of the ion and neutral reactant, respectively. At the lowest energies, the ion energies are corrected for truncation of the ion beam as described previously.[33] CD_4 gas (99% isotopically pure) was obtained from Cambridge Isotope Laboratory. The CD_4 reactant gas was subjected to multiple freeze−pump−thaw cycles to remove any noncondensable impurities. Removal of residual oxygen is particularly important in this study because WO^+ has the same mass as $[W,C,2D]^+$, and the reactions forming these isobaric ions both occur at low kinetic energies.

Ion Source. W^+ and $[W,C,2H]^+$ ions are made in a dc discharge/flow tube (DC/FT) source described in detail previously.[31] For this study, $^{186}W^+$ (30.67% natural abundance) was used in the $W^+ + CH_4$ (CD_4) systems and $^{182}W^+$ (26.3% natural abundance) was used for $[W,C,2H]^+ + H_2$ (D_2). The DC/FT source utilizes a tungsten cathode held at 1.0−1.7 kV over which a flow of approximately 90% He and 10% Ar passes at a typical pressure of 0.5−0.6 mTorr. The tungsten cathode was either a rod supported by an iron holder or wire wrapped around the iron holder. Both forms of the tungsten cathode gave similar intensities of W^+ ions. Ar^+ ions created in the direct current discharge are accelerated toward the tungsten cathode, sputtering off atomic metal ions. To quench any excited states of W^+ and to generate $[W,C,2H]^+$, we add a small amount of methane to the flow gases about 60 cm downstream of the source. Methane pressures are kept low to minimize secondary reactions of $[W,C,2H]^+$, which decrease the ion intensity. The ions undergo $>10^4$ collisions with the flow gases as they traverse the flow tube and therefore are expected to be at room temperature. Reactant ions are extracted from the flow tube and focused through a 9.5 cm long differentially pumped region before entering the rest of the instrument described above. Before any reactions of $[W,C,2H]^+$ were conducted, a high-energy collision-induced dissociation (CID) spectrum of the $[W,C,2H]^+$ with Xe was collected to ensure that no unexpected product ions were observed. On the basis of the threshold measured for this CID reaction, no evidence for the presence of excited ions was observed, as discussed further below.

Previous studies in our group have shown that the DC/FT source generates atomic metal ions with electronic temperatures ranging from 300 to 1100 K.[34−38] W^+ has a ^6D ground state with five spin−orbit levels, $J = {}^1/_2-{}^9/_2$, having excitation energies of 0.000, 0.188, 0.393, 0.585, and 0.762 eV and a ^6S first excited state at 0.920 eV.[39] Assuming an average electronic temperature of 700 K, the fractions of ions in each level are 0.9150, 0.0807, 0.0040, 0.0002, 0.0000, and 0.0000, respectively. Therefore, the ions are believed to be in the ground electronic state term and largely in the lowest spin−orbit level. From the populations of ions at 700 ± 400 K, the average electronic energies are calculated to be 0.017 (+0.040/−0.017) eV for W^+. These estimated populations are consistent with the failure to observe any obvious evidence for electronically excited M^+ species in the present and related studies.[40]

Thermochemical Analysis. For endothermic reactions, the threshold energy can be obtained by analyzing the product cross section with

$$\sigma(E) = \sigma_0 \Sigma g_i (E + E_{\mathrm{el}} + E_i - E_0)^n / E \qquad (1)$$

where σ_0 is an energy-independent scaling parameter, E is the relative translational energy of the reactants, E_{el} is the average electronic energy of the tungsten ions (see above), n is a variable parameter that controls the shape of the cross section, and E_0 is the 0 K threshold for reaction of ground electronic, vibrational, and rotational state reactants. The summation is over the rovibrational states of the reactants having relative populations g_i ($\Sigma g_i = 1$) and energies E_i. Average rovibrational energies of the reactants at 300 K are 0.040 and 0.044 eV for $W^+ + CH_4$ and $W^+ + CD_4$, respectively.[28] Before comparison with the data, the model of eq 1 is convoluted over the neutral and ion kinetic energy distributions using previously developed methods.[33] The parameters E_0, σ_0, and n are optimized using a nonlinear least-squares analysis to best reproduce the data. Reported values of E_0, σ_0, and n are mean values for each parameter from the best fits to several sets of data. Uncertainties are one standard deviation from the mean. The listed uncertainties in the E_0 values also include the uncertainties in the absolute energy scale and internal energies of the reactants.

Theoretical Approach. Most of the quantum chemistry calculations reported here are computed using the B3LYP hybrid density functional method[41,42] and performed with the GAUSSIAN 98 suite of programs.[43] The B3LYP functional was used for most calculations because it provided reasonable results for the analogous Re^+ and $Pt^+ + CH_4$ systems[13,14] and was also the choice of Simon et al.[9] Because several of the transition states of interest here involve bridging hydrogens, a large basis set is used for carbon and hydrogen, triple-ζ with diffuse and polarization functions, 6-311++G(3df,3p). This basis set gives good results for the thermochemistry of methane and dihydrogen, with deviations from experiment of less than 0.08 eV for the bond energies of $H-CH_3$ (4.406 vs 4.480 eV), H_2-CH_2 (4.666 vs 4.713 eV), H−CH (4.332 vs 4.360 eV), C−H (3.532 vs 3.465 eV), and H−H (4.505 vs 4.478 eV). (See Table 1 of ref 28 for thermochemistry used for all H, D, CH_x, and CD_x species.) The 60 core electrons of tungsten are described by the relativistic effective core potentials (ECPs) of Hay-Wadt (HW),[44] equivalent to the Los Alamos double-ζ ECP (LANL2DZ) basis set. The HW-ECP is optimized for neutral atoms, whereas the positive charge differentially contracts the s orbitals compared to the d orbitals. Hence, all calculations were performed with an altered HW-ECP basis for W as described by Ohanessian et al. (HW+).[45] Harmonic frequencies of the normal modes were determined and zero-point vibrational energies were evaluated at the B3LYP/HW+/6-311++G(3df,3p) level of theory. In all cases, the thermochemistry calculated here is corrected for zero point energies after scaling the calculated frequencies by 0.989.[46]

The most appropriate level of theory has been thoroughly investigated for the first- and third-row transition metal methyl cations by Holthausen et al.[12] and for first-row transition metal methylene cations by Holthausen, Mohr, and Koch.[47] In the first study, these authors used B3LYP, Becke-Half-and-Half-LYP (BHLYP), and QCISD(T) methods with a basis set consisting of a polarized double-ζ basis on C and H and the Hay/Wadt relativistic ECP with valence electrons added. For the first-row MCH_3^+ species (M = Sc to Cu), where experimental results are available for all metals,[24,27] these authors conclude that the B3LYP functional overbinds severely, with a mean absolute

deviation (MAD) from experiment of 0.41 eV. The BHLYP functional and the QCISD(T) methods perform more accurately, with MADs of 0.18 and 0.20 eV, respectively. For the third-row elements, the bond energies calculated using B3LYP were again higher than those for BHLYP and QCISD(T), whereas for the metal methylene complexes,[47] the performance of the B3LYP functional is quite good and the BHLYP functional predicts bond energies consistently below experimental values. On the basis of these results, the present study utilizes primarily the B3LYP functional (as most species investigated have more than a single covalent bond to W^+), but we also performed calculations for the ground states of the various product ions using the BHLYP functional, along with QCISD(T) calculations. For comparison, the B3P86[41,48] and MPW1PW91[49] functionals were also investigated. Such calculations will be explicitly noted, but unless otherwise designated, our results will refer to a B3LYP/HW+/6-311++G(3df,3p) level of theory. For most species, spin contamination was not observed to be a problem; however, several of the low-spin states exhibited evidence for spin contamination, and these cases will be noted explicitly below.

In all cases, the experimental BDEs refer to the ground spin−orbit state at 0.0 eV: $a^6D_{1/2}$ for W^+.[39] In contrast, because the calculations do not explicitly include spin−orbit interactions, any calculated thermochemistry involving an asymptote including W^+ is referenced to the properly weighted mean of all spin−orbit levels in the ground state term: 0.514 eV for $W^+(a^6D)$.[39] A proper comparison between the experimental and calculated BDEs should therefore includes corrections for this different asymptotic energy, as well as spin−orbit effects in the molecular species, where the latter are generally unknown. If it is assumed that spin−orbit coupling is largely quenched for all molecular species containing tungsten, then the theoretical values should be reduced by the 0.514 eV average energy. Such a simple correction is clearly an approximation and an overestimation, especially as Simon et al. have calculated the spin−orbit stabilization of $WCH_2^+(^4A'')$, $HWCH^+(^2A')$, and $WCH^+(^3\Delta)$ as 0.06, 0.15, and 0.29 eV, respectively.[9] In our theoretical bond energies for W^+-CH_x reported below, we report the value obtained without any spin−orbit corrections, as well as a value approximately corrected by including the spin−orbit energy of W^+ (0.514 eV) coupled with an estimate for the spin−orbit energy of the tungsten-containing molecular ion. For WCH^+ and WCH_2^+, we use the calculated values of Simon et al.[9] For WH^+, WC^+, and WCH_3^+, we approximate the spin−orbit corrections as equivalent to those for WCH^+ (for the linear WH^+ and WC^+ species) or WCH_2^+ (for WCH_3^+ which also has C_s symmetry).

Results

$W^+ + CH_4$, CD_4. As shown in Figure 1, reaction of $W^+ + CH_4$ (CD_4) yields five product ions formed in reactions 2−6.

$$W^+ + CH_4\,(CD_4) \rightarrow WCH_3^+\,(WCD_3^+) + H\,(D) \quad (2)$$

$$\rightarrow [W,C,2H]^+\,([W,C,2D]^+) + H_2\,(D_2) \quad (3)$$

$$\rightarrow WCH^+\,(WCD^+) + H_2\,(D_2) + H\,(D) \quad (4)$$

$$\rightarrow WC^+ + 2\,H_2\,(D_2) \quad (5)$$

$$\rightarrow WH^+\,(WD^+) + CH_3\,(CD_3) \quad (6)$$

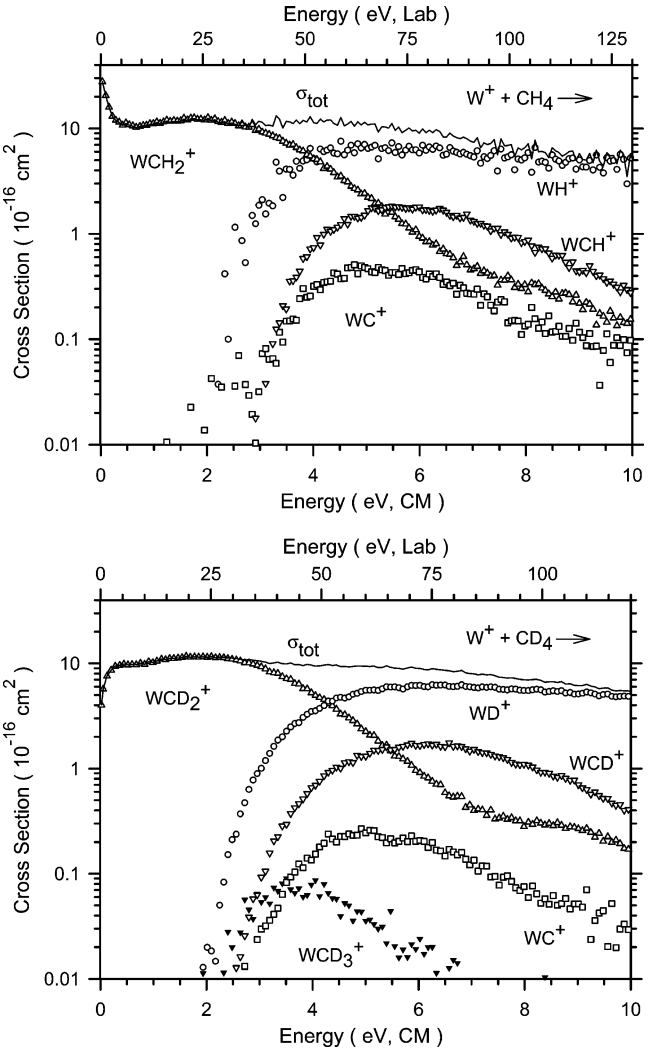

Figure 1. Cross sections for reactions of W^+ with CH_4 (at 0.15 mTorr, part a) and with CD_4 (at 0.28 mTorr, part b) as a function of kinetic energy in the center-of-mass (lower axis) and laboratory (upper axis) frames.

Reactions for CH_4 and CD_4 are qualitatively very similar with two exceptions. First, the energy dependence of reactions 3 below 0.5 eV differ in the two systems, a result that is discussed in detail below. Second, WCH_3^+ is not observed because of its much smaller (2 orders of magnitude) intensity relative to the $[W,C,2H]^+$ product ion. The product of reaction 2 can be seen in the CD_4 system because of the larger mass separation between WCD_3^+ and $[W,C,2D]^+$. In all cases, some overlap of adjacent masses was observed but because of the differing energy dependences of the product ions, corrections for such mass overlap could be made unambiguously.

Dehydrogenation of methane to form $[W,C,2H]^+$ ($[W,C,2D]^+$), reaction 3, is the dominant reaction below 2 eV. Near 2.5 eV, the $[W,C,2H]^+$ cross section begins to decline rapidly. Such behavior can result from decomposition or competition with formation of another product. $[W,C,2H]^+$ can decompose by losing CH_2 to form W^+ starting at 4.71 eV $= D_0(H_2-CH_2)$,[28] by dehydrogenation to form WC^+, or by losing H to form WCH^+. The first pathway is too energetic and the latter two pathways have insufficient intensity to explain the decline observed in the $[W,C,2H]^+$ cross section. Therefore, competition with reaction 6 must account for this decline. Evidence for this conclusion is that the decline in the $[W,C,2H]^+$ ($[W,C,2D]^+$) cross section is compensated by the increase in the WH^+ (WD^+)

cross section, such that the total cross section varies smoothly with energy, Figure 1. This competition indicates that these two products share a common intermediate.

The WH^+ (WD^+) cross section rises from an apparent threshold near 2 eV and plateaus above about 5 eV. The WCD_3^+ cross section rises from a threshold similar to WD^+ but reaches a maximum magnitude near 4 eV. This behavior cannot be explained by dissociation to $W^+ + CD_3$, which cannot begin until 4.58 eV = $D_0(D-CD_3)$.[28] Instead, the decline is attributed to subsequent dehydrogenation of this product to form WCD^+. This product cross section has an apparent threshold near 2.5 eV and reaches its maximum at about 6 eV. This is probably a result of decomposition of its precursor, WCD_3^+, to $W^+ + CD_3$, as formation of $W^+ + CD + D_2 + D$ requires 9.25 ± 0.04 eV.[28] WCD_3^+ also decomposes by D atom loss to form $[W,C,2D]^+$, evident as the second feature in the $[W,C,2D]^+$ cross section, which becomes apparent near 7 eV. As this second feature is also observed in the $[W,C,2H]^+$ cross section, the intermediacy of WCH_3^+ is confirmed, even though this product is not observed for reasons noted above. The fact that this process is observed even though dehydrogenation is a much lower energy channel indicates that H (D) atom loss is kinetically more favorable than H_2 (D_2) elimination. WC^+, which begins at about 2.5 eV, must be formed in reaction 5 by dehydrogenation of $[W,C,2H]^+$ ($[W,C,2D]^+$). The cross section of WC^+ begins to decline near 5 eV probably because the $[W,C,2H]^+$ ($[W,C,2D]^+$) precursor decomposes to $W^+ + CH_2$ (CD_2).

Multiple Collision Dehydrogenation Reactions. The primary $[W,C,2H]^+$ and $[W,C,2D]^+$ products formed in reactions 3 react further with methane. We observed that W^+ successively dehydrogenates eight methane molecules, to form a sequence of $WC_xH_{2x}^+$, $x = 1-8$, product ions. The first five products are shown in Figure 2a, where the intensities of the last three products ($x = 6-8$) were similar to one another and 20 times smaller than that for $WC_5H_{10}^+$. The energy dependences indicate that each of these subsequent reactions are exothermic and have no barriers in excess of the reactants' energies. These results agree well with observations of Irikura and Beauchamp.[1,2] They observed that W^+ reacts rapidly four times with methane with rates of 1.2, 3.0, 2.4, and 1.0 × 10^{-10} cm^3 s^{-1} to form $[W,C,2H]^+$, $WC_2H_4^+$, $WC_3H_6^+$, and $WC_4H_8^+$, respectively, and subsequent reactions occur slowly as far as $WC_8H_{16}^+$.

The reactivity of W^+ with CD_4 observed here is less extensive, Figure 2b. The formation of secondary products observed is rapid, similar to the CH_4 system, but the rate for the formation of $[W,C,2D]^+$ is slow, as noted above. Similar results were reported by Irikura and Beauchamp when they used $^{13}CD_4$.[2] Sequential reactions of W^+ with CD_4 lead to $[W,C,2D]^+$, $WC_2D_4^+$, $WC_3D_6^+$, and $WC_4D_8^+$ with rate constants of <0.1, 3.4, 2.2, and 0.7 × 10^{-10} cm^3 s^{-1}, respectively, but no higher order products were observed.

Because $[W,C,2H]^+$ ($[W,C,2D]^+$) reacts so efficiently with CH_4 (CD_4), the shape of the cross section for this primary product is very sensitive to the pressure used. As shown in Figure 3, the $[W,C,2H]^+$ cross sections decrease with increasing pressure as more $WC_xH_{2x}^+$ ($x \geq 2$) products are formed. For the perprotio system, the total cross sections, $\Sigma\sigma(WC_xH_{2x}^+)$, are essentially identical at all pressures, Figure 3a. When the cross sections of $[W,C,2H]^+$ are extrapolated to zero pressure of the methane reactant, a cross section consistent with the total cross sections is found. Therefore, the total cross section can be regarded as the $[W,C,2H]^+$ cross section when no secondary products are formed, i.e., under rigorously single collision

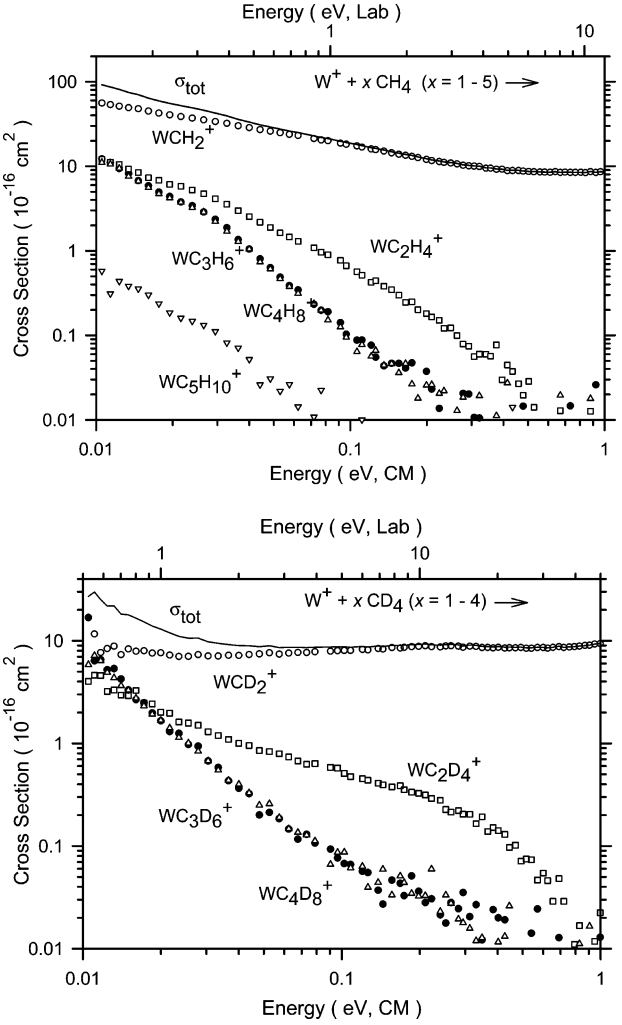

Figure 2. Cross sections for the successive dehydrogenation reactions of W^+ with CH_4 (at 0.023 mTorr, part a) and with CD_4 (at 0.037 mTorr, part b) as a function of kinetic energy in the center-of-mass (lower axis) and laboratory (upper axis) frames.

conditions. This cross section varies with energy as $E^{-0.6}$ from 0.01 to 0.5 eV, comparable to the $E^{-0.5}$ energy dependence predicted by the collision model of Langevin−Gioumousis−Stevenson (LGS),[50] but having a magnitude about one-third of the LGS cross section at the lowest energies. Our cross section values can also be converted to rate constants for the comparison with the ICR studies. Microcanonical rate constants are related to cross sections by $k(\langle E\rangle) = v\sigma(v)$, where $v = (2E/\mu)^{1/2}$ is the nominal relative velocity of the reactants, $\mu = Mm/(m + M)$ is the reduced mass of the reactants, $\langle E\rangle = E + 3\gamma k_B T/2$, $\gamma = M/(m + M)$, k_B is Boltzmann's constant, and T is the temperature of the methane molecule. Because the guided ion beam technique allows very low ion energies, the rate constant at room temperature, $k(T)$, can be obtained directly from the data at low energies.[33] (In essence, at the lowest collision energies, the interaction energy is dominated by the motion of the neutral reactant, such that the data are actually more representative of $k(T)$ than $\sigma(E)$. Also, because the cross sections vary approximately as $E^{-0.5}$, the $k(\langle E\rangle)$ values vary little with energy such that an average over a Maxwell−Boltzmann distribution of velocities yields the same value for $k(T)$.) At 300 K, the rate constant for formation of $[W,C,2H]^+$ from our zero pressure extrapolated data is (2.0 ± 0.4) × 10^{-10} cm^3 s^{-1}. Although this value is slightly larger than (1.2 ± 0.3) × 10^{-10} cm^3 s^{-1} reported in the ICR study,[2] this latter value may be somewhat low

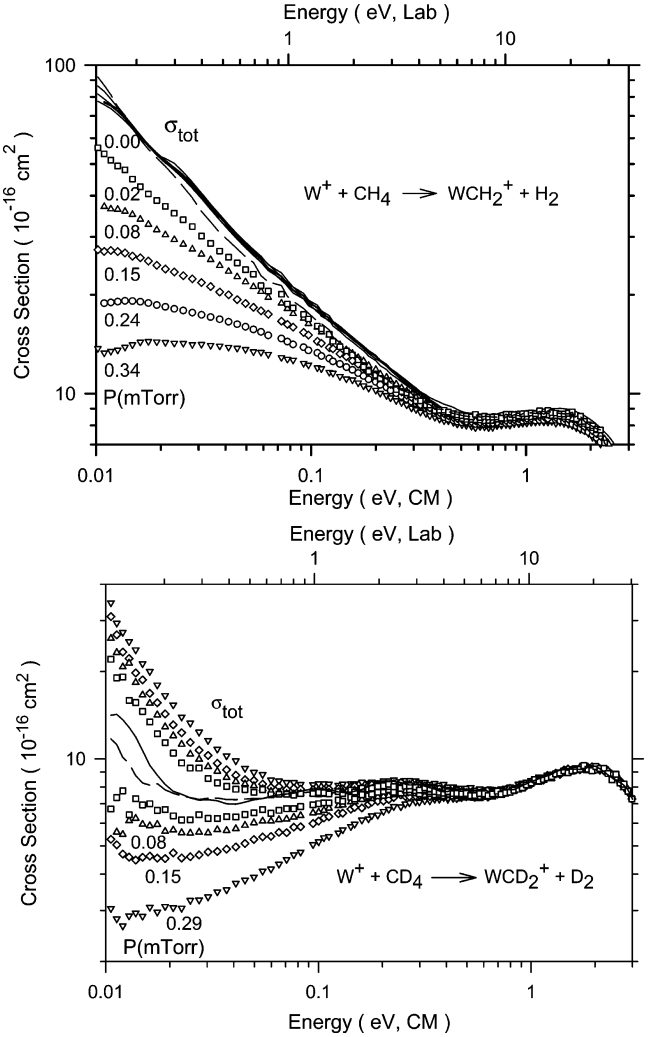

Figure 3. Primary products and total cross sections for the dehydrogenation reactions of W^+ with CH_4 and CD_4 as a function of kinetic energy in the center-of-mass (lower axis) and laboratory (upper axis) frames. Part a shows results for the reaction of $W^+ + CH_4$ with 0.023 (squares), 0.083 (triangles), 0.153 (diamonds), 0.243 (circles), and 0.335 (inverted triangles) mTorr of CH_4. Full lines show the total cross sections at all five pressures, whereas the dashed line shows the product cross sections extrapolated to zero pressure. Part b shows results for the reaction of W^+ with 0.037 (squares), 0.075 (triangles), 0.146 (diamonds), and 0.294 (inverted triangles) mTorr of CD_4. Lower symbols show $[W,C,2D]^+$ cross sections, whereas upper symbols show the total cross sections at each pressure. In part b, the dashed and full lines show the primary products and total cross sections extrapolated to zero pressure, respectively.

because of the perturbations explicitly observed here for the fast secondary reactions. These rate constants can be compared to the LGS collision rate of 9.8×10^{-10} cm^3 s^{-1}.

Similar results hold for the CD_4 system although here the $[W,C,2D]^+$ cross sections decrease and the total cross sections increase in magnitude with increasing pressure, Figure 3b. When the $[W,C,2D]^+$ and $\Sigma\sigma(WC_xD_{2x}^+)$ cross sections are extrapolated to zero pressure of methane, they agree well above 0.02 eV and they are within the absolute uncertainty of ±20% below 0.02 eV. The thermal rate constant of $[W,C,2D]^+$ obtained from our zero pressure extrapolated cross section is $0.35 \pm 0.07 \times 10^{-10}$ cm^3 s^{-1}, again somewhat larger than $<0.1 \times 10^{-10}$ cm^3 s^{-1} reported in the ICR study,[2] which again may be suppressed by the subsequent reactions. The observation that the total reaction cross section increases with increasing pressure is unusual behavior that is presumably driven by the very reactive

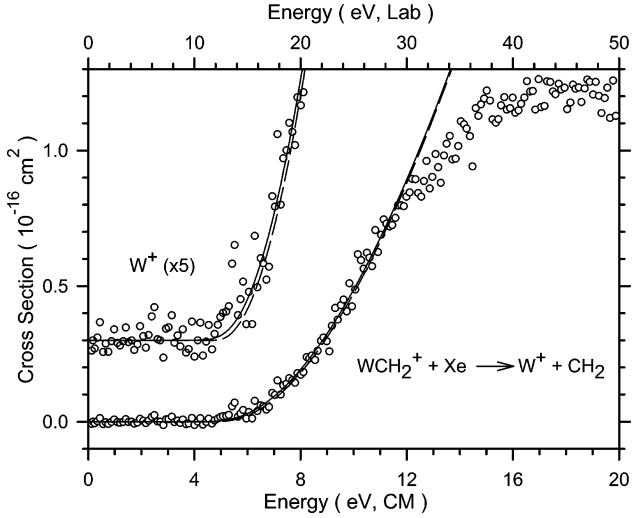

Figure 4. Cross section for reaction of $[W,C,2H]^+$ with Xe as a function of kinetic energy in the center-of-mass (lower axis) and laboratory (upper axis) frames. The estimated 0 K cross section for formation of W^+ is shown by the broken line. The full line shows the cross section after convolution over the neutral and ionic kinetic and internal energy distributions.

secondary products. Apparently, some of the $W^+ + CD_4$ collisions that do not form $[W,C,2D]^+$ under single collision conditions can lead to $WC_xD_{2x}^+$ production at higher pressures. This is plausibly attributed to translational cooling which permits the reactant ions to have long residence times in the collision region.

$[W,C,2H]^+ + Xe$. Collision-induced dissociation of $[W,C,2H]^+$ with Xe yields only the W^+ product in abundance, as shown in Figure 4.

$$[W,C,2H]^+ + Xe \rightarrow W^+ + CH_2 + Xe \qquad (7)$$

This contrasts with the photodissociation results of Simon et al. who find loss of H beginning above 2.5 eV.[9] Our failure to observe this process is because detection of WCH^+ and WC^+ products in this experiment is very difficult in our instrument, a consequence of the enormous difference in intensities of the reactant and product ions (especially at threshold) along with the mass resolution in the analysis quadrupole mass filter being especially limited on the low mass side of the very intense $[W,C,2H]^+$ reactant ion. Unfortunately, use of $[W,C,2D]^+$ as the reactant ion is prohibitively expensive because of the large amounts of gas needed in the flow tube source to generate these species. The cross section for reaction 7 rises beginning near 5 eV and plateaus above about 15 eV. The measured threshold, 4.9 ± 1.0 eV (Table 1) has a large uncertainty reflecting the slow rise in the cross section. This value agrees with the lower limit of 4.71 ± 0.03 eV established by the exothermicity of the dehydrogenation reaction of CH_4, process 3.

$[W,C,2H]^+ + H_2$ and D_2. To further characterize the WCH_4^+ system, we examined the reverse of the dehydrogenation reaction. Reactions of $[W,C,2H]^+$ with H_2 and D_2 were studied and exhibited reactions 8−11 below 0.3 eV, Figure 5.

$$[W,C,2H]^+ + H_2 \rightarrow W^+ + CH_4 \qquad (8)$$

$$[W,C,2H]^+ + D_2 \rightarrow W^+ + CH_2D_2 \qquad (9)$$

$$\rightarrow [W,C,H,D]^+ + HD \qquad (10)$$

$$\rightarrow [W,C,2D]^+ + H_2 \qquad (11)$$

TABLE 1: Parameters of Eq 1 Used in Modeling the Reaction Cross-sections

reactants	products	σ_0 (Å^2 eV^{1-n})	n	E_0 (eV)	$D_0(W^+-L)$ (eV)
$W^+ + CH_4$	$WH^+ + CH_3$	13.3 ± 4.0	1.0 ± 0.4	2.86 ± 0.28	>1.62 ± 0.28
	$WC^+ + 2\,H_2$	0.95 ± 0.40	1.1 ± 0.5	3.10 ± 0.35	4.96 ± 0.35
	$WCH^+ + H_2 + H$	2.17 ± 0.95	1.5 ± 0.4	2.90 ± 0.31	6.17 ± 0.31
	$[W,C,2H]^+ + H_2$[a]	6.43 ± 0.17	1.1 ± 0.4	0.55 ± 0.10	4.16 ± 0.10
$W^+ + CD_4$	$WD^+ + CD_3$	9.55 ± 3.30	1.2 ± 0.3	2.86 ± 0.23	>1.72 ± 0.23
	$WC^+ + 2\,D_2$	0.72 ± 0.24	1.0 ± 0.5	3.24 ± 0.28	4.96 ± 0.28
	$WCD^+ + D_2 + D$	3.41 ± 0.71	1.1 ± 0.2	3.27 ± 0.15	5.98 ± 0.15
	$[W,C,2D]^+ + D_2$[b]	7.18 ± 1.30	0.8 ± 0.3	0.071 ± 0.025	4.75 ± 0.03
	a	6.36 ± 1.10	1.3 ± 0.4	0.68 ± 0.17	4.14 ± 0.17
	$WCD_3^+ + D$[c]	2.03 ± 0.94	1.6 ± 0.4	2.82 ± 0.27	>1.76 ± 0.27
$[W,C,2H]^+ + Xe$	$W^+ + CH_2 + Xe$	0.17 ± 0.22	2.4 ± 0.7	4.9 ± 1.0	4.9 ± 1.0

[a] Feature corresponding to excited state of the $[W,C,2H]^+$ ($[W,C,2D]^+$) product. See text. [b] Feature corresponding to ground state of the $[W,C,2D]^+$ product. See text. [c] Measured by analysis of the sum of the $WCD_3^+ + WCD^+$ cross sections.

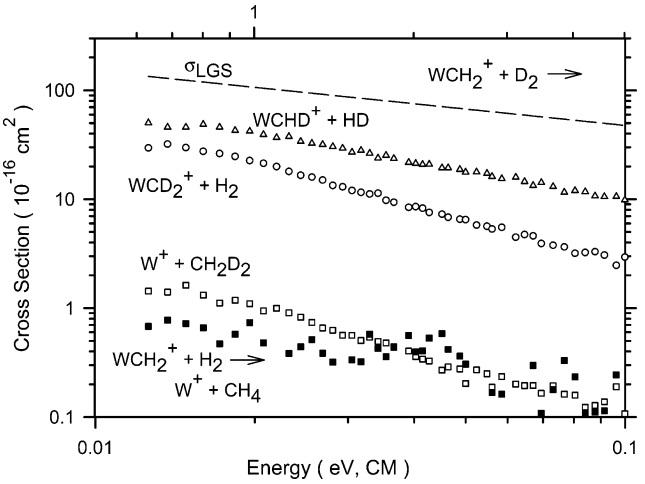

Figure 5. Cross sections for the reaction of $[W,C,2H]^+ + D_2$ (open symbols) and $[W,C,2H]^+ + H_2$ (closed symbols) as a function of kinetic energy in the center-of-mass (lower axis) and laboratory (upper axis) frames. The dashed line shows the LGS collision cross section.

Other reactions are likely at higher energies but were not examined here. Clearly, the hydrogen scrambling reactions 10 and 11 are much more probable than the pathway going to $W^+ + CH_2D_2$. The hydrogen scrambling reactions 10 and 11 are slightly exothermic given the zero point energy differences between reactants and products (by 0.02 and 0.06 eV, respectively, according to the theoretical frequencies calculated here). The cross section for W^+ formed in reaction 9 is slightly more intense and declines a little more rapidly than the cross section for reaction 8. This is because zero point energy differences make reaction 9 more favorable than reaction 8 by 0.08 eV. In Figure 5, these cross sections are compared to the Langevin−Gioumousis−Stevenson (LGS) collision cross section.[50] Only the cross section for reaction 8 declines as $E^{-0.5}$, whereas the cross sections for reactions 9−11 in the $[W,C,2H]^+ + D_2$ system decline as $E^{-0.8}$ ($E^{-1.3}$ above 0.02 eV), $E^{-0.9}$, and $E^{-1.3}$, respectively.

As shown in Figures 1 and 3, dehydrogenation of CH_4 by W^+ shows no barriers in excess of the reactant energy, implying an exothermic process. The reverse processes 8 and 9 also do not exhibit obvious barriers to reaction, although they are much less efficient than reactions 3. These observations indicate that processes 8 and 9 must be slightly endothermic. To further quantify the thermochemistry of these reactions, we determine the equilibrium constant for reaction 8 and its reverse, reaction 3, $K_{eq} = k_f(8)/k_r(3)$. Because the neutral reagents are characterized by room-temperature energy distributions, the equilibrium determination corresponds to 298 K, where we find $k_f(8)/k_r(3) = 0.033 \pm 0.011$.

To convert this equilibrium constant to thermodynamic information, we use the equations, $\Delta G_{298} = -RT \ln K_{eq}$, $\Delta H_{298} = \Delta G_{298} + T\Delta S_{298}$ and $\Delta H_0 = \Delta H_{298} - \Delta[H_{298} - H_0]$. Here, S_{298} and $[H_{298} - H_0]$ values for H_2 (130.68 ± 0.03 J K^{-1} mol^{-1}, 8.467 kJ mol^{-1}), CH_4 (186.24 ± 0.04 J K^{-1} mol^{-1}, 10.024 kJ mol^{-1}), and W^+ (179.74 ± 0.08 J K^{-1} mol^{-1}, 6.221 kJ mol^{-1}) are taken from the NIST-JANAF Thermodynamic Tables.[51] For $[W,C,2H]^+$, these values (271.6 ± 0.5 J K^{-1} mol^{-1}, 10.8 kJ mol^{-1}) are calculated using standard statistical mechanical functions starting with the molecular parameters calculated here. Thus, our experimental equilibrium constant yields a 298 K free energy for reaction 8 of 0.09 ± 0.01 eV, a 298 K enthalpy of −0.02 ± 0.01 eV, and a 0 K enthalpy of 0.01 ± 0.01 eV.

In the hydrogen scrambling reactions 10 and 11, the magnitude of the cross section for $[W,C,2D]^+$ is smaller than that of $[W,C,H,D]^+$, by a factor of 1.65 ± 0.15 at the lowest energy studied and by larger amounts at increasing energies. An estimate for the cross section representing a return to reactants (formation of $[W,C,2H]^+ + D_2$) can be obtained by subtracting the observed product cross sections from the total σ_{LGS} collision cross section. This yields a cross section comparable to that for $[W,C,H,D]^+ + HD$ at low energies (<0.02 eV) and remaining relatively flat at higher energies. Thus, at low energies, the branching ratio for production of $[W,C,2H]^+ + D_2$, $[W,C,H,D]^+ + HD$, and $[W,C,2D]^+ + H_2$ channels is approximately 38:38:23%. Using free energies at 298 K calculated here for these product channels, we predict that an equilibrium distribution should have ratios of 48:37:15%, in reasonable agreement with experiment. This agreement substantiates the equilibrium approach used above to derive thermochemistry for reaction 8.

Thermochemical and Theoretical Results

The cross sections for the endothermic processes 2 and 4−6 for both perprotio and perdeutero methane as well as reaction 3 for CD_4 are analyzed with eq 1, and the optimized parameters are listed in Table 1. The measured thresholds for the CH_4 and CD_4 systems are shifted from one another because of zero point energy differences but are in generally good agreement.

The bond dissociations energies (BDEs) of W^+ bound to H and CH_x, $x = 0-3$, can be derived from the reaction thresholds assuming that the threshold represents the energy of the product asymptote using the relation, $D_0(W^+-L) = D_0(R-L) - E_0$, where RL is CH_4 or CD_4. This assumption is usually correct for ion−molecule reactions because of the long-range attractive forces. Because all sources of energy are included in our modeling using eq 1, the thermochemistry obtained corresponds to 0 K values.[27] The BDEs obtained from the thresholds are listed in Table 1 for both CH_4 and CD_4 reactants and are summarized in Table 2.

TABLE 2: Comparison of Experimental and Theoretical Bond Energies (eV) for WH^+ and WCH_x^+ ($x = 0-3$) Species

	this work						previous work	
		theory[a]						
species	exp	B3LYP	BHLYP	B3P86	MPW1PW91	QCISD(T)	exp	theory
W^+-H ($^5\Delta$)	2.27 ± 0.05[b]	2.42 (2.64)	2.23 (2.45)	2.44 (2.66)	2.16 (2.38)	2.21 (2.43)		2.16[c]
W^+-CH_3 (^5A)	$\sim 2.31 \pm 0.10$	2.59 (3.04)	2.18 (2.63)	2.75 (3.20)	2.52 (2.97)	2.67 (3.13)		2.18 ± 0.22[d]
								2.15 ± 0.22[d]
W^+-CH_2 ($^4A''$)	4.73 ± 0.06	4.38 (4.84)	3.66 (4.11)	4.53 (4.99)	4.15 (4.60)	4.55 (5.00)	>4.71[e]	4.29[f]
								(4.81 ± 0.22)[f]
								4.84[g]
WCH^+-H ($^4A''$)	3.08 ± 0.29	2.79 (3.03)	2.94 (3.17)	3.38 (3.62)	2.97 (3.20)	3.08 (3.31)	2.5 ± 0.1[g]	2.51−2.85[g]
$H-WCH^+$ ($^2A'$)		2.77 (2.92)		2.85 (2.99)	2.62 (2.77)	3.20 (3.35)		
W^+-CH ($^3\Delta$)	6.01 ± 0.28	5.92 (6.14)	5.03 (5.25)	5.74 (5.96)	5.68 (5.90)	5.71 (5.93)	6.6 ± 0.1[g]	6.03[h]
W^+-C ($^2\Delta$)	4.96 ± 0.22	4.66 (4.88)	3.70 (3.92)	4.80 (5.02)	4.36 (4.58)	4.06 (4.28)[i]		

[a] Calculations using the level of theory indicated with a 6-311++G(3df,3p) basis set on C and H and the Hay−Wadt[44] basis set for W as adjusted for the cation by Ohanessian et al.[45] Values have been corrected for spin−orbit energies of W^+ and the WCH_x^+ molecule (see text), whereas values in parentheses are the directly calculated values. [b] Reference 40. [c] References 11 and 45. [d] Reference 12. [e] Reference 2, corrected to 0 K from 298 K. [f] Reference 10. Value in parentheses is the recommended value. [g] Reference 9. [h] Estimated in ref 10. [i] $^2\Sigma^+$ ground state at this level of theory.

Theoretical results for each of the product ions are also provided. Table 2 lists BDEs calculated at several levels of theory. More extensive B3LYP calculations are given in Table 3, which summarizes the energetics of these product ions and their low-lying excited states, and Table 4, which lists geometric information for all these species. Ground state structures are shown in Figure 6.

W^+-H. The BDEs of WH^+ (WD^+) have been measured in the reaction of $W^+ + H_2$ (D_2), $D_0(W^+-H) = 2.25 \pm 0.06$ eV and $D_0(W^+-D) = 2.32 \pm 0.06$ eV, giving an average after zero point energy corrections of $D_0(W^+-H) = 2.27 \pm 0.05$ eV.[40] This BDE predicts that the thermodynamic thresholds for reactions 6 with CH_4 (CD_4) are 2.21 ± 0.05 eV (2.27 ± 0.05 eV), whereas our measured thresholds are much higher, 2.86 ± 0.28 eV (2.86 ± 0.23 eV). Apparently, the threshold values for reactions 6 are shifted to higher values because of strong competition with reactions 3. Indeed, a phase space theory calculation using molecular parameters (vibrational and rotational constants) calculated here finds a competitive shift in approximate accord (within 0.1 eV) with that needed to explain the observed behavior in the WH^+ (WD^+) cross sections. In the $W^+ + H_2$ (D_2) reactions, there are no competitive channels, such that more reliable thermochemistry is obtained.

The BDE for WH^+ of 2.27 ± 0.05 eV agrees nicely with the theoretical value of 2.16 eV from Goddard and co-workers.[11,45] Our computed values depend heavily on the level of theory used. Excellent agreement with experiment is found for the BHLYP, MPW1PW91, and QCISD(T) values that include spin−orbit stabilization corrections (an adjustment of $0.22 = 0.514-0.295$ eV), Table 2. As found by Holthausen et al.,[12] B3LYP tends to overbind somewhat, and B3P86 behaves similarly. If no spin−orbit correction is applied, then all levels of theory explored here exceed the experimental value by 0.1−0.4 eV, Table 2.

As discussed previously,[45] theory finds three states for WH^+, $^5\Pi$, $^5\Delta$, and $^5\Sigma^+$, which differ primarily in their occupied 5d nonbonding orbitals, $\sigma\pi\delta^2$, $\sigma\pi^2\delta$, and $\pi^2\delta^2$, respectively. GVB calculations find a $^5\Pi$ ground state, with a $^5\Delta$ state lying only 0.07 eV higher in energy.[45] Our B3LYP calculations invert this order with the $^5\Delta$ state as the ground state, lying only 0.006 eV lower than the $^5\Pi$ state, Table 3. Spin−orbit coupling could alter the ordering of these states, such that an unambiguous assignment of the true ground state for WH^+ cannot be made. Both GVB and B3LYP calculations also find an excited $^5\Sigma^+$ state lying about 0.20 eV above the respective ground states. The GVB calculations show that the WH^+ molecule involves covalent bond formation between a singly occupied sd hybridized orbital on W^+ (59% 5d and 40% 6s) and the singly occupied 1s orbital on H.[45]

W^+-CH_3. Because of the much larger intensity of the $[W,C,-2H]^+$ product ion, a cross section for the WCH_3^+ product ion formed in reaction 2 could not be measured reliably. The better mass separation afforded by deuterium substitution permits this product cross section to be determined in the CD_4 reaction system, but the observation that it decomposes readily into WCD^+ means that the sum of the WCD_3^+ and WCD^+ cross sections is analyzed using eq 1. The resulting threshold lies slightly below that measured for reaction 6. Because the formation of WCD_3^+ should compete with $[W,C,2D]^+$ formation at least as much as WD^+ and also must compete with the more favorable WD^+ channel as well, the threshold obtained from this analysis is presumed to be an upper limit to the thermodynamic value. After a zero-point energy correction of 0.013 eV, we obtain a lower limit of 1.77 ± 0.27 eV for $D_0(W^+-CH_3)$. If we assume that the $WD^+ + CD_3$ and $WCD_3^+ + D$ channels are similarly affected by competition with $[W,C,2D]^+$, then the relative thresholds of the WD^+ and WCD_3^+ channels can be used to provide our best estimate of the WCH_3^+ bond energy as 0.04 eV above $D_0(W^+-H)$, yielding $\sim 2.31 \pm 0.10$ eV.

Holthausen et al. have thoroughly investigated the first- and third-row transition metal methyl cations using B3LYP, BHLYP, QCISD, and QCISD(T) levels of theory.[12] With the geometry held to C_{3v}, they obtained W^+-CH_3 bond energies of 2.71, 2.39, 1.92, and 1.99 eV, respectively, without zero point energy corrections or adjustments for the spin−orbit levels. On the basis of results for first-row metal methyl cations compared to experiment, Holthausen et al. applied empirical corrections of −0.22 and +0.16 eV to their BHLYP and QCISD(T) results, leading to final suggested bond energies of 2.18 and 2.15 eV with estimated errors of ±0.22 eV. These values are in reasonable agreement with our adjusted experimental value of ~2.31 eV, and well above the uncorrected value of 1.77 eV, suggesting that the former is more likely to be correct. Our computed bond energies at the B3LYP, BHLYP, and QCISD(T) levels are 3.04, 2.63, and 3.13 eV after correcting for zero point energies, well above the results of Holthausen et al. The stronger bonds found here are probably because of the difference in ground state geometries, as discussed further below. After an approximate correction for the spin−orbit stabilization (0.514−0.06 eV), these bond energies shift to 2.59, 2.18, and

TABLE 3: Theoretical Energies of Reactants and Products Calculated at the B3LYP/HW+/6-311++G(3df,3p) Level of Theory

species	state	energy (E_h)	ZPE (E_h)[a]	E_{rel} (eV)[b]
H	^2S	−0.502257		
H_2	$^1\Sigma_g^+$	−1.180030	0.009953	
C	^3P	−37.857442		
CH	$^2\Pi$	−38.495898	0.006369	0.000
	$^4\Sigma$	−38.462172	0.006867	0.931
CH_2	$^3B_1$	−39.167949	0.016980	
CH_3	$^2A''$	−39.857664	0.029358	
CH_4	$^1A_1$	−40.536527	0.044035	
W^+	^6D	−67.345887		0.000
	^6S	−67.326103		0.538
	^4F	−67.314176		0.863
	^2X	−67.295075		1.383
WH^+	$^5\Delta$	−67.949656	0.004611	0.000
	$^5\Pi$	−67.949383	0.004563	0.006
	$^5\Sigma^+$	−67.942913	0.004426	0.178
WC^+	$^2\Delta$	−105.384878	0.002368	0.000
	$^4\Delta$	−105.373140	0.002392	0.320
	$^4\Sigma^-$	−105.363396	0.002352	0.584
	$^4\Pi$	−105.349884	0.002019	0.943
	$^2\Sigma^+$	−105.350132	0.002366	0.945
	$^6\Pi$	−105.342020	0.002017	1.154
WCH^+	$^3\Delta$	−106.074099	0.013054	0.000
	$^3\Sigma^-$	−106.055435	0.011110	0.455
	$^1\Gamma$	−106.045076	0.012863	0.785
HWC^+	$^3A'$	−105.983993	0.008379	2.325
	$^1A'$	−105.982871	0.008719	2.364
	$^1A''$	−105.982207	0.008442	2.375
	$^3A''$	−105.978364	0.008319	2.476
WCH_2^+	$^4A''$	−106.695499	0.020958	0.000
	$^4A_2$ (TS)[c]	−106.690418	0.020033 (262i)	0.113
	$^2A''$	−106.679767	0.020853	0.425
	$^4B_1$	−106.677576	0.021880	0.513
	$^4B_2$	−106.677179	0.021879	0.524
	$^6A_1$	−106.668782	0.021858	0.751
	$^2A'$	−106.646337	0.025340	1.457
	$^6B_1$	−106.585544	0.019809	2.961
$HWCH^+$	$^2A'$	−106.689861	0.019412	0.111
	$^2A''$	−106.680553	0.019222	0.359
WCH_3^+	^5A	−107.317462	0.032101	0.000
	$^5A'$	−107.316659	0.032069	0.021
	$^5A''$ (TS)[d]	−107.315708	0.031456 (659i)	0.030
	$^3A'$	−107.293086	0.032103	0.663
	$^3A''$	−107.282833	0.031200	0.918
TS	^3A	−107.280259	0.027849 (1055i)	0.897
$HWCH_2^+$	^3A	−107.309023	0.027914	0.116
H_2WCH^+	$^1A'$	−107.308232	0.027018	0.113

[a] Zero point energy. Scaled by 0.989. Imaginary frequencies are listed in cm^{-1}. [b] Energy relative to the ground state species for each compound including zero point energies (scaled by 0.989). [c] Collapses to $^4A''$ state. [d] Collapses to ^5A state.

2.67 eV, respectively, where the BHLYP value is in good agreement with experiment and the adjusted values of Holthausen et al. B3P86 and MPW1PW91 appear to perform similarly to B3LYP in this case, Table 2. In any case, these results and those of Holthausen et al. demonstrate that the B3LYP level of theory systematically overestimates the bond energies of the transition metal methyl cations, whereas BHLYP performs reasonably well.

Holthausen et al. find that the ground state of WCH_3^+ is ^5E with C_{3v} symmetry imposed, whereas our ground state is ^5A with a geometry close to having C_s symmetry. Explicit calculations of $^5A'$ and $^5A''$ states find these lie 0.02 and 0.03 eV higher in energy, respectively, although the latter state has one imaginary frequency corresponding to rotation of the methyl group about an axis perpendicular to the W−C bond. The bond lengths of W−C (2.02 Å) and C−H, 1.09 (2) and 1.12 (1) Å, and WCH bond angles, 91° (1) and 116° (2), are distinct from the C_{3v} geometries calculated by Holthausen et al. (2.12 Å, 1.10 Å, and 110°, B3LYP; 2.14 Å, 1.10 Å, and 111°, QCISD(T)).[12] Notably the W−C bond is shorter, consistent with the stronger binding found in our calculations, and one of the hydrogens leans toward the tungsten, Figure 6. We also find an excited $^3A'$ state of WCH_3^+ lying 0.663 eV higher in energy, Table 3. (This state exhibited evidence for spin contamination with $S^2 = 2.89$ instead of 2.0.) A $^3A''$ state lies 0.918 eV above the ground state.

The reason for the strong distortions from C_{3v} symmetry observed in this system is illustrated by the existence of stable alternate geometries, namely $HWCH_2^+$ and H_2WCH^+, Figure 6. The former species, a hydridotungsten carbene, has three covalent bonds to tungsten such that it has a triplet ground state. This species is actually lower in energy than the WCH_3^+ ($^3A'$) geometry by 0.55 eV, but still higher than the WCH_3^+ (^5A) ground state by 0.12 eV, Table 3. Interconversion of these species on the triplet surface requires surmounting a barrier 0.23 eV above WCH_3^+ ($^3A'$) and 0.78 eV above $HWCH_2^+$ (^3A). On the quintet surface, the $HWCH_2^+$ geometry lies about 1.15 eV above the WCH_3^+ ground state but collapses to the WCH_3^+ geometry. There is also a stable dihydridotungsten carbyne, H_2WCH^+, which has five covalent bonds to tungsten such that it has a singlet ground state. This species lies only 0.11 eV higher than the WCH_3^+ (^5A) species, Table 3, whereas the singlet $HWCH_2^+$ geometry lies 0.65 eV higher in energy but collapses to H_2WCH^+. Clearly, the ability of tungsten to form multiple bonds allows facile rearrangement of the WCH_3^+ cation.

[W,C,2H]$^+$. The formation of $[W,C,2H]^+$ in reaction 3 is exothermic, indicating $D_0(W^+-CH_2) > 4.71 \pm 0.03$ eV, as previously concluded by Irikura and Beauchamp.[2] From the 0 K enthalpy of reaction 8, 0.01 ± 0.01 eV, obtained by measurement of the equilibrium constant, we determine $D_0(W^+-CH_2) = 4.72 \pm 0.04$ eV. The formation of $[W,C,2D]^+$ in reaction 3 is endothermic by 0.07 ± 0.03 eV, Table 1 and Figure 7, such that $D_0(W^+-CD_2) = 4.75 \pm 0.03$ eV. After correction for isotopic differences of 0.014 eV, this yields a 0 K bond energy for W^+-CH_2 of 4.74 ± 0.03 eV, in good agreement with the value obtained from the equilibrium constant. We take the weighted average of these two values as our best measure of this bond energy with two standard deviations of the mean as the uncertainty, yielding $D_0(W^+-CH_2) = 4.73 \pm 0.06$ eV. Note that this value indicates that reaction 3 with CH_4 is exothermic at 0 K by 0.02 ± 0.06 eV and reaction 3 with CD_4 is endothermic by 0.08 ± 0.06 eV. These results are in agreement with the behavior of the data of Figures 1 and 3 as well as the equilibrium results.

A very extensive theoretical investigation of the geometries and states of the $[W,C,2H]^+$ molecule has been conducted by Simon et al.[9] They used several basis sets, the largest of which is called 3, and they also explored B3LYP, CCSD(T), and CASPT2 levels of theory as well as estimating spin−orbit corrections. Our B3LYP theoretical results essentially reproduce their B3LYP/3 results including geometries in all details and relative energies of all states within a couple of kJ/mol. Because of the extensive discussion of these results and their comparison to the previous results of Irikura and Goddard,[10] where the geometry was restricted to C_{2v}, we will not revisit these results in detail. However, it is useful to note that the same structural flexibility observed above for the WCH_3^+ molecule was also found for $[W,C,2H]^+$. Thus, the $^4A_2$ state found by Irikura and Goddard has an imaginary frequency such that it collapses to the distorted $^4A''$ species shown in Figure 6 and lying 0.42 eV

TABLE 4: Theoretical Structures of Reactants and Products Calculated at the B3LYP/HW+/6-311++G(3df,3p) Level of Theory[a]

species	state	r(W−H)	r(W−C)	r(C−H)	∠WCH	∠HW(C,H)	∠HCH	∠dihedral
CH	$^2\Pi$			1.122				
	$^4\Sigma$			1.093				
CH_2	$^3B_1$			1.078			135.1	
CH_3	$^2A''$			1.078(3)			120.0(3)	
CH_4	$^1A_1$			1.088(4)			109.5(6)	
WH^+	$^5\Delta$	1.671						
	$^5\Pi$	1.692						
	$^5\Sigma^+$	1.702						
WC^+	$^2\Delta$		1.687					
	$^4\Delta$		1.732					
	$^4\Sigma^-$		1.720					
	$^4\Pi$		1.792					
	$^2\Sigma^+$		1.724					
	$^6\Pi$		1.842					
WCH^+	$^3\Delta$		1.726	1.085	180.0			
	$^3\Sigma^-$		1.738	1.084	180.0			
	$^1\Gamma$		1.732	1.085	180.0			
HWC^+	$^3A'$	1.704	1.734			104.8		
	$^1A'$	1.680	1.676			91.4		
	$^1A''$	1.676	1.725			90.1		
	$^3A''$	1.707	1.731			104.8		
WCH_2^+	$^4A''$	1.934	1.793	1.082, 1.168	78.4, 167.2		114.3	180.0
	$^4A_2$ (TS)		1.841	1.094(2)	122.0(2)		116.0	180.0
	$^2A''$	1.878	1.777	1.083, 1.193	75.6, 170.8		113.6	180.0
	$^4B_1$		1.876	1.093(2)	123.0(2)		114.1	180.0
	$^4B_2$		1.875	1.093(2)	122.9(2)		114.1	180.0
	$^6A_1$		2.023	1.091(2)	123.0(2)		114.1	180.0
	$^2A'$	1.951	1.789	1.082, 1.164	79.7, 165.4		114.9	180.0
	$^6B_1$		2.002	1.090(2)	105.0(2)		150.0	180.0
$HWCH^+$	$^2A'$	1.681	1.723	1.085	176.9	89.1 (C)		0.0
	$^2A''$	1.677	1.727	1.085	176.3	90.2 (C)		180.0
WCH_3^+	^5A		2.020	1.091(2), 1.122	91.4, 116.2(2)		108.0(2), 113.9	±118.2
	$^5A'$		2.004	1.090(2)	86.5		107.7(2)	±118.2
				1.132	117.9(2)		114.2	
	$^5A''$ (TS)		2.003	1.090	105.8		106.2	±123.8
				1.102(2)	114.8(2)		111.9(2)	
	$^3A'$		1.976	1.090(2)	79.4		107.5(2)	±118.1
				1.153	119.8(2)		114.5	
	$^3A''$		1.929	1.092(2)	74.2		108.1(2)	±117.6
				1.191	120.6(2)		114.7	
TS	^3A	1.735	1.891	1.091	58.6, 120.5, 124.8	52.8 (C)	114.7	83.9, −95.1
				1.094				
$HWCH_2^+$	^3A	1.668	1.790	1.082	78.7	91.1 (C)	114.4	70.5, −98.2
				1.168	166.5			
H_2WCH^+	$^1A'$	1.676(2)	1.723	1.085	176.0	94.3 (H)		±47.2
						89.4 (2,C)		

[a] Bond lengths are in Å. Bond angles are in degrees. Degeneracies are listed in parentheses.

lower in energy. Three excited states all having C_{2v} symmetry, $^4B_1$, $^4B_2$, and $^6A_1$, lie 0.51, 0.52, and 0.75 eV higher in energy than the $^4A''$ ground state. The lowest excited state found was a $^2A''$ state (not discussed by Simon et al. perhaps because it has spin contamination, $S^2 = 1.57$ instead of 0.75) lying 0.42 eV above the $^4A''$ state. As for the WCH_3^+ species, migration of a hydrogen atom from the carbon to tungsten can occur yielding stable $HWCH^+$ species having $^2A'$ and $^2A''$ states. Without spin−orbit corrections, these states lie 0.11 and 0.36 eV higher than the $^4A''$ state, but Simon et al. find that the spin−orbit correction for the $HWCH^+$ ($^2A'$) state is −0.15 eV, +0.09 eV for the $HWCH^+$ ($^2A''$) state, and −0.06 for the WCH_2^+ ($^4A''$) state. Thus, our calculations indicate that $HWCH^+$ ($^2A'$) lies only 0.02 eV above WCH_2^+ ($^4A''$) once this correction has been made, whereas Simon et al. find relative energies after spin−orbit correction of 0.01 (B3LYP/3), −0.05 (CCSD(T)/3), and −0.07 (CASPT2/3) eV. Further, Simon et al. find the barrier for conversion between the WCH_2^+ ($^4A''$) and $HWCH^+$ ($^2A'$) states (including SO corrections) is 0.56−0.65 eV, as confirmed by the present calculations. Interestingly, we found that the interconversion of WCH_2^+ and $HWCH^+$ on the $^2A''$ excited state surface (where both geometries represent minima) basically parallels the combined adiabatic WCH_2^+ ($^4A''$)/$HWCH^+$ ($^2A'$) surfaces but lies 0.2−0.3 eV higher in energy throughout.

Our measured value for $D_0(W^+-CH_2)$ agrees well with the value recommended by Irikura and Goddard, 4.81 ± 0.22 eV,[10] although this includes an empirical correction of 0.52 eV to a directly calculated value of 4.29 eV. In the work of Simon et al.,[9] an explicit calculation of the W^+-CH_2 bond energy is not given but these authors note that their CCSD(T)/3 results indicate that reaction 3 is exothermic by 0.17 eV. This exothermicity corresponds to a bond energy of 4.84 eV using an appropriate theoretical value for $D_0(H_2-CH_2)$ to calculate this BDE. Our calculations, Table 2, find BHLYP results severely underestimate the BDEs of multiply bonded transition metal species, as found previously.[13,14,47] Likewise the MPW1PW91 value is also somewhat low, whereas the B3LYP, B3P86, and QCISD(T) calculations provide bond energies that are in reasonable agreement with experiment. Directly calculated values tend to be higher than experiment, Table 2, whereas those approximately corrected for spin−orbit stabilization (0.514−0.06 eV) lie somewhat below. Given the results above for the

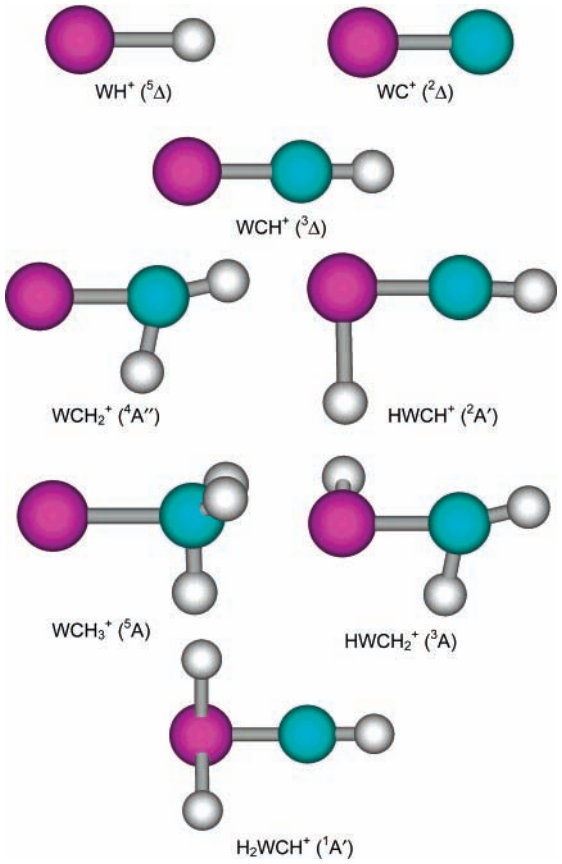

Figure 6. Structures of the ground states for WH^+ and WCH_x^+ ($x = 0-3$) calculated at the B3LYP/HW+/6-311++G(3df,3p) level of theory.

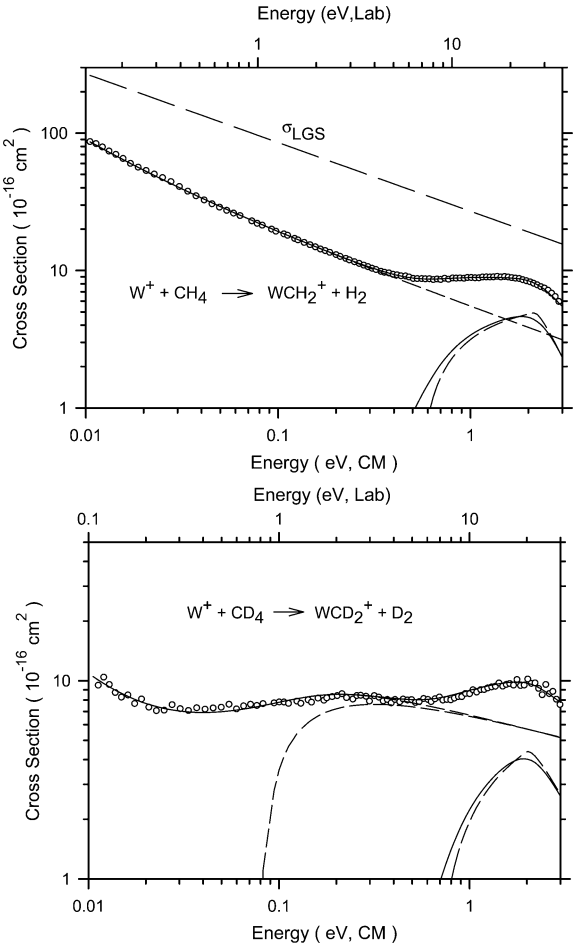

Figure 7. Zero pressure cross sections for $[W,C,2H]^+$ (part a) and $[W,C,2D]^+$ (part b) formation in reactions of $W^+ + CH_4$ and $W^+ + CD_4$ as a function of kinetic energy in the center-of-mass (lower axis) and laboratory (upper axis) frames. The estimated 0 K cross sections for formation of ground and excited states of $[W,C,2H]^+$ and $[W,C,2D]^+$ are shown by the dashed lines. The full lines show these cross sections and their sums after convolution over the experimental energy distributions. The long dashed line in part a shows the LGS collision cross section.

relative energies of the WCH_2^+ ($^4A''$) and $HWCH^+$ ($^2A'$) states, these comparisons are unaltered by considering the latter species instead.

$[W,C,2H]^+$ Excited State. The cross sections of both $[W,C,2H]^+$ and $[W,C,2D]^+$ exhibit a second feature at higher energies, most obvious in Figure 3. Analyses of these features (after accounting for the low-energy cross sections) are shown in Figure 7 and yield thresholds of 0.55 ± 0.10 and 0.68 ± 0.17 eV, respectively, Table 1. This corresponds to $[W,C,2H]^+$ species having bond energies of $D_0(W^+-CH_2) = 4.16 \pm 0.10$ eV and 4.13 ± 0.17 eV, respectively, where the latter value has been corrected for zero point energy differences. The weighted average of these values is 4.15 ± 0.17 eV, where the uncertainty is two standard deviations of the mean. This corresponds to an excited state of $[W,C,2H]^+$ lying 0.58 ± 0.18 eV above the ground state.

The excitation energy of 0.58 ± 0.18 eV can be compared to theoretical results. This value is between 0.23 eV for $^4B_1$ and 0.95 eV for $^6A_2$ states of WCH_2^+ calculated by Irikura and Goddard, in which several low-lying electronic states are reported.[10] Our calculations find $^2A''$, $^4B_1$, $^4B_2$, and $^6A_1$ states of WCH_2^+ in the right energy range, 0.42, 0.51, 0.52, and 0.75 eV, respectively, as well as a $^2A''$ state of $HWCH^+$ at 0.36 eV. Excluding the WCH_2^+ ($^2A''$) state, Simon et al. find similar excitation energies at the B3LYP/3 level and somewhat higher values (0.68, 0.77, 0.92, and 0.40 eV, respectively) at the CCSD-(T)/3 level.

W^+-CH. From analysis of reactions 4, the BDEs for WCH^+, 6.17 ± 0.31 eV, and WCD^+, 5.98 ± 0.15 eV, can be obtained. As the correction for isotopic substitution is negligible, 0.002 eV, the weighted average of these two values, 6.01 ± 0.28 eV, is taken as our best determination of $D_0(W^+-CH)$, with an uncertainty given by two standard deviations of the mean. Remarkably, this bond energy agrees almost exactly with the estimate of 6.03 eV made by Irikura and Goddard,[10] who developed a value for the intrinsic strength of the triple W−C bond and then corrected by exchange and promotion energies. Likewise, theoretical results at the B3LYP, B3P86, MPW1PW91, and QCISD(T) levels give reasonable agreement with experiment, whereas the BHLYP value is again low by about one electronvolt.

In contrast to this good agreement, the various theoretical values all lie well below the W^+-CH bond energy suggested by the experiments of Simon et al., 6.6 ± 0.1 eV.[9] This value is derived using their experimental photodissociation measurement of the WCH^+-H bond energy of 2.5 ± 0.1 eV combined with experimental values for $D(W^+-CH_2)$ and $D(HC-H)$.[9] Alternatively, this comparison can be made by noting that the experimental thermochemistry derived here provides the WCH^+-H bond energy as 3.08 ± 0.29 eV. The calculations of Simon et al. obtain a BDE for H atom loss from WCH_2^+ of 3.04 eV at their B3LYP/3 and CCSD(T)/3 levels of theory and a somewhat lower value of 2.74 eV at the CASPT2/3 level. If a spin−orbit correction of 0.23 eV (0.29−0.06 eV as appropriate for the WCH_2^+ geometry) is also included, the predicted BDEs

drop to 2.81 (B3LYP/3 and CCSD(T)/3) and 2.51 eV (CASPT2/3). (One could also consider the $HWCH^+$ species, for which the $H-WCH^+$ bond energy is calculated to be 2.79 (B3LYP/3), 2.85 (CCSD(T)/3), and 2.58 (CASPT2/3) including a spin−orbit correction of 0.15 eV (0.295−0.15 eV). As noted above, it is unclear whether WCH_2^+ ($^4A''$) or $HWCH^+$ ($^2A'$) is the most stable geometry, such that the bond energies for H atom loss do not change appreciably no matter which species is considered.) Overall, the values calculated by Simon et al. range from 2.51 to 2.85 eV with spin−orbit adjustments, and from 2.73 to 3.04 eV without them. The lowest values agree better with the experimental results of Simon et al., whereas the higher values agree better with our experimental results. Our calculations at the B3LYP level reproduce the B3LYP/3 results of Simon et al., giving a BDE for H atom loss from WCH_2^+ ($^4A''$) of 3.03 eV, whereas other levels of theory give higher values by 0.14−0.59 eV. Spin−orbit corrected values range from 2.79 to 3.38 eV and agree better with the present experimental results. Our calculations indicate that the $H-WCH^+$ ($^2A'$) BDE ranges from 2.62 to 3.20 eV including spin−orbit corrections, Table 2, leading to the same qualitative conclusions. It is possible that our experimental bond energy for W^+-CH is too low although the WCH^+ product is not actually competing with other product channels because it is formed primarily by decomposition of the primary and dominant $[W,C,2H]^+$ product. As noted by Simon et al.,[9] it is possible that their photodissociation threshold is too low because their ions are not completely thermalized.

The calculations of Simon et al. find a ground state for WCH^+ of $^3\Delta$ with a $^3\Sigma$ state lying between 0.36 (CASPT2/3) and 0.67 (CCSD(T)/3) eV higher in energy depending on the level of theory. Our B3LYP calculations reproduce these results including the geometries for both states and an excitation energy of 0.46 eV, Table 3, in good agreement with the B3LYP/3 results of Simon et al. The leading valence electronic configurations of these two states are $(\sigma_b)^2(\pi_b)^4(\delta)^1(\sigma)^1$ and $(\sigma_b)^2(\pi_b)^4(\delta)^2$, where the σ_b and π_b orbitals are W−C bonding orbitals, the σ and δ orbitals are metal-based nonbonding, and the C(2s) valence electrons are not explicitly indicated for simplicity. We also located an excited singlet state, 0.78 eV above the $^3\Delta$ ground state, also having the $(\sigma_b)^2(\pi_b)^4(\delta)^2$ configuration and therefore assigned to a $^1\Gamma$ state. (Perhaps not surprisingly, this state has some spin contamination, $S^2 = 1.0$ instead of 0.0.) All three of these states have very similar linear geometries, Table 4, consistent with a covalent triple bond in each with only variations in the nonbonding orbital populations.

Because of the structural variations observed for the WCH_3^+ and WCH_2^+ molecules, we also examined the HWC^+ structure. In this case, both singlet and triplet species are located but are found to lie 2.3−2.5 eV above the WCH^+ ($^3\Delta$) ground state, Table 3. Both the W−H and W−C bond lengths are comparable to those found in WH^+ and WC^+, indicating that the covalency of the bonds is maintained. That both singlet and triplet states are close in energy is consistent with covalent coupling of the H atom to the $^2\Delta$ ground and $^4\Delta$ low-lying states of WC^+.

W^+-C. Double dehydrogenation of CH_4 and CD_4 requires 8.06 and 8.20 eV, respectively.[28] From the thresholds for reaction 5, Table 1, we obtain bond energies of 4.96 ± 0.35 and 4.96 ± 0.28 eV, respectively. We assign the latter value as our best determination of this bond energy. This value agrees reasonably with our bond energies calculated at the B3LYP and B3P86 levels whether corrected for spin−orbit stabilization (0.514−0.295 eV) or not, Table 2. Values calculated at the MPW1PW91 and QCISD(T) levels are low and BHLYP is about 1 eV too low, similar to the results for $[W,C,2H]^+$.

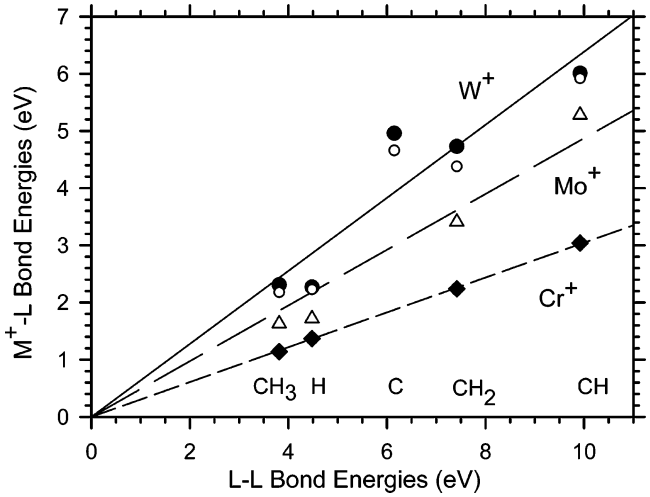

Figure 8. Correlation of W^+-L (closed circles), Mo^+-L (open triangles, refs 24 and 35), and Cr^+-L (closed diamonds, refs 52−55) bond energies with those for the organic analogues L−L. Lines are linear regression fits to the experimental data constrained to pass through the origin. Theoretical values (open circles) for W^+-L are also shown, BHLYP/HW+/6−311++G(3df,3p) for WH^+ and WCH_3^+ and B3LYP/HW+/6-311++G(3df,3p) for all others.

Theory finds a ground state for WC^+ of $^2\Delta$, with excited states of $^4\Delta$, $^4\Sigma^-$, $^4\Pi$, $^2\Sigma^+$, and $^6\Pi$ lying 0.32, 0.58, 0.94, 0.94, and 1.15 eV higher in energy. (Uniquely among these states, the $^2\Delta$ state shows spin contamination, $S^2 = 1.40$ instead of 0.75.) These states have leading valence electron configurations of $(\sigma_b)^2(\pi_b)^4(\delta)^1$, $(\sigma_b)^1(\pi_b)^4(\delta)^1(\sigma)^1$, $(\sigma_b)^1(\pi_b)^4(\delta)^2$, $(\sigma_b)^2(\pi_b)^3(\delta)^2$, $(\sigma_b)^1(\pi_b)^4(\delta)^2$, and $(\sigma_b)^1(\pi_b)^3(\delta)^2(\sigma)^1$, where the character of the molecular orbitals is comparable to those of WCH^+ and the C(2s) electrons are again not explicitly given. Bond lengths increase for each of these states, accurately reflecting the number of occupied bonding orbitals, which indicate that the approximate bond order is 3, 2.5, 2.5, 2.5, 2.5, and 2, respectively. $C(^3P)$ forms a triple bond in the $^2\Delta$ state of WC^+ in the same way it does in CO, namely by accepting a pair of electrons into the empty 2p orbital.

Given that the approximate bond order of the WC^+ ($^2\Delta$) and WCH^+ ($^3\Delta$) ground states are both 3, it is reasonable to ask why the bond energy of WC^+, 4.96 ± 0.28 eV, is more like that of WCH_2^+, 4.73 ± 0.06 eV, than WCH^+, 6.01 ± 0.28 eV. Formation of the $WCH^+(^3\Delta)$ triple bond can occur by coupling $W^+(^6D)$ + $CH(^4\Sigma)$ with a promotion energy of 0.72 for $CH(^4\Sigma)$. To form the covalent triple bond in the $^2\Delta$ state of WC^+, W^+ must be promoted from its ^6D ground state to its $^4D(6s^15d^4(^5D))$ excited state, lying 1.32 eV higher in energy (using the statistical average of the spin−orbit states).[39] Further, the calculations suggest that the σ_b molecular orbital has much more 6s character in the WC^+ molecule, making the overlap with C(2p) less effective for bonding. Overall, the difference in the required promotion energies (0.6 eV) and the less effective σ bond appears to account for the difference in the WC^+ and WCH^+ bond energies.

Bond-Energy Bond-Order Correlation for W^+-CH_x Bonds. Figure 8 shows the correlation of W^+-L bond energies with those for the organic analogues L−L. A linear regression analysis of the data shows a remarkably good correlation. (This line is constrained to include the origin to emphasize the bond−order correlation of the WL^+ vs L_2 species.) This correlation suggests that W^+-H and W^+-CH_3 are single bonds, $W^+=CH_2$ is a double bond, and $W^+\equiv CH$ is a triple bond, all in agreement with theoretical characterizations as well. The point that lies furthest from the line is for W^+-C, which is compared

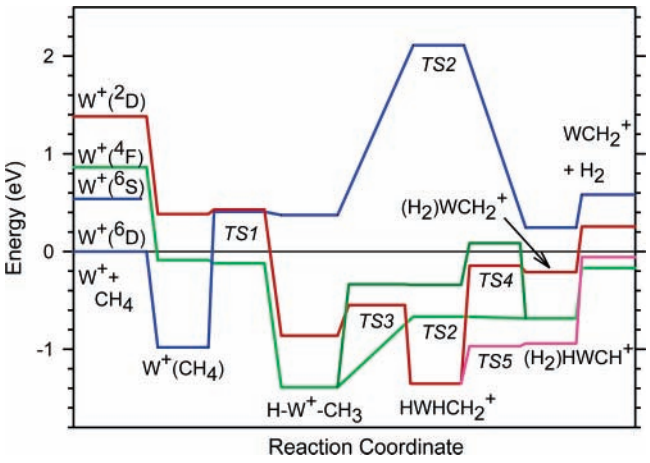

Figure 9. $[W,C,4H]^+$ potential energy surfaces derived from theoretical results. The relative energies of all species are based on ab initio calculations (B3LYP/HW+/6-311++G(3df,3p); see Tables 3 and 5). Energies are relative to the W^+ (^6D) + CH_4 ground state asymptote with zero point energy but no spin−orbit corrections included. Sextet surfaces are shown in blue, quartet surfaces in green (TS2) and dark green (TS3 and TS4), and doublet surfaces in red (TS4, WCH_2^+ pathway) and pink (TS5, $HWCH^+$ pathway).

with the BDE of C_2. In this case, the W^+−C BDE is stronger than predicted by this simple correlation because the covalent double bond in the WC^+ molecule is augmented by back-donation of an occupied 5d orbital on W^+ into the empty 2p orbital on C. Such an interaction cannot occur in the C_2 molecule. Also illustrated in Figure 8 is the relatively good agreement between experiment and theory: B3LYP/HW+ for multiply bonded species and BHLYP/HW+ for the singly bonded species.

The enhanced reactivity of W^+ compared with its congeners, Cr^+ and Mo^+, is clearly illustrated by the relative BDEs, as shown in Figure 8. $D_0(Cr^+-H) = 1.37 \pm 0.09$ eV,[27,52] $D_0(Cr^+-CH_3) = 1.14 \pm 0.03$ eV,[27,53,54] $D_0(Cr^+-CH_2) = 2.24 \pm 0.04$ eV,[27,54,55] $D_0(Cr^+-CH) = 3.04 \pm 0.30$ eV,[27,54] and $D_0(Mo^+-H) = 1.72 \pm 0.06$ eV[35] are taken from previously published studies. $D_0(Mo^+-CH_3) = 1.63 \pm 0.12$ eV, $D_0(Mo^+-CH_2) = 3.41 \pm 0.12$ eV, and $D_0(Mo^+-CH) = 5.28 \pm 0.10$ eV are preliminary values from our laboratory.[24]

All of the BDEs for Cr^+ and Mo^+ are smaller than those of W^+, which can be explained by considering promotion energies and s- and d-orbital sizes.[2,11,13,14] The ground state of W^+ is $6s^15d^4$ (^6D), a configuration suitable for forming a strong single covalent bond as well as multiple covalent bonds. To reach this same configuration, Cr^+ and Mo^+ have promotion energies from their ^6S (d^5) ground states to ^6D (s^1d^4) excited states of 1.48 and 1.46 eV, respectively. In W^+, relativistic effects cause the 6s orbital to shrink so that its radial extent closely matches that of the 5d orbitals, thereby allowing more effective hybridization of these orbitals. Irikura and Beauchamp reported that the orbital size differences between valence *s*- and d-orbitals decrease from Cr^+ to Mo^+ to W^+.[2] This helps explain why Mo^+ shows stronger bond strengths than Cr^+, even though promotion energies are similar for Cr^+ and Mo^+.

Potential Energy Surfaces of $[W,C,4H]^+$

The potential energy surfaces for interaction of W^+ with methane are shown in Figure 9. All energies were calculated at the B3LYP/HW+/6-311++G(3df,3p) level of theory and include zero point energy corrections (scaled by 0.989). In most cases, transition states were located using the synchronous transit-guided quasi-newton method (QST3)[56,57] followed by geometry optimizations and frequency calculations to verify a first-order saddle point. As suggested above, the B3LYP level of theory overbinds species with single covalent bonds to W^+ but appears to handle multiple bonds adequately. As nearly all of the species on these surfaces involve several bonds to W^+, the relative characteristics of the surfaces are likely to be qualitatively correct. Even if the energetics are not quantitative, the qualitative characteristics of the surfaces are of the most interest here. Tables 5 and 6 provide summaries of the theoretical results (energies and structures) for each of the intermediates and transition states. None of the sextet or quartet species exhibit spin contamination.

TABLE 5: Theoretical Energies of $[W,C,4H]^+$ Intermediates and Transition States Calculated at the B3LYP/HW+/6-311++G(3df,3p) Level of Theory

species	state	energy (E_h)	ZPE (E_h)[a]	E_{rel} (eV)[b]
$W^+(^6D) + CH_4$		−107.882414	0.044035	0.000
$W^+(CH_4)$	$^6A_1$	−107.917938	0.043514	−0.981
	^4A	−107.885707	0.044125	−0.087
	^4A (TS)[c]	−107.885641	0.043184 (113i)	−0.111
	$^4A_2$ (TS)[c]	−107.885448	0.043086 (200i)	−0.108
	$^4A_1$	−107.885276	0.044103	−0.076
	$^4A_2$	−107.874374	0.042986	0.190
	^2A	−107.867797	0.043548	0.384
	$^2A_1$	−107.860490	0.043517	0.582
TS1	$^6A'$	−107.860494	0.037064 (217i)	0.406
	$^4A'$	−107.883116	0.040631 (530i)	−0.112
	^2A	−107.863886	0.040699 (393i)	0.413
$HWCH_3^+$	$^6A'$	−107.862243	0.037580	0.373
	^4A	−107.927472	0.037993	−1.390
	^4A (TS)[d]	−107.893481	0.035711 (1083i)	−0.528
	^2A	−107.909303	0.038275	−0.888
	$^2A''$ (TS)[e]	−107.906652	0.037950 (163i)	−0.825
	$^2A'$	−107.898336	0.039223	−0.564
TS2	$^6A'$	−107.790328	0.029523 (275i)	2.111
	$^4A'$	−107.898831	0.035961 (617i)	−0.666
TS3	^4A	−107.885209	0.034470 (160i)	−0.336
	$^2A''$	−107.893430	0.034909 (381i)	−0.548
$(H)_2WCH_2^+$	$^4A''$	−107.885653	0.034722	−0.341
	$^4A'$	−107.844779	0.034165	0.756
	$^2A'$	−107.923883	0.035770	−1.353
	^2A (TS)[f]	−107.920457	0.035151 (273i)	−1.277
	^2A	−107.923595	0.035914	−1.342
	$^2A'$ (TS)[g]	−107.918601	0.034277 (232i)	−1.250
	$^2A''$ (TS)[e]	−107.867891	0.034609 (240i)	0.139
TS4	$^4A''$	−107.869079	0.033859 (1197i)	0.086
	^2A	−107.877844	0.034124 (637i)	−0.145
$(H_2)WCH_2^+$	$^6A'$	−107.865461	0.036076	0.245
	$^4A''$	−107.899750	0.036181	−0.685
	^2A	−107.882499	0.035708	−0.229
	$^2A''$ (TS)[h]	−107.882471	0.035453 (45i)	−0.235
TS5	^2A	−107.907222	0.033546 (746i)	−0.960
$(H_2)HWCH^+$	^2A	−107.908130	0.035494	−0.932
	$^2A'$	−107.880499	0.031368	−0.293
	$^2A''$ (TS)[h]	−107.873972	0.032391 (199i)	−0.087
$(H_2)HWCH^+$(planar)	$^2A'$	−107.883641	0.032896	−0.336
	$^2A''$	−107.875393	0.033118	−0.106
$WCH_2^+ + H_2$	$^6A_1$	−107.848812	0.031811	0.582
	$^4A''$	−107.875529	0.030911	−0.170
	$^2A''$	−107.859797	0.030806	0.255
$HWCH^+ + H_2$	$^2A'$	−107.869891	0.029365	−0.058

[a] Zero point energy. Scaled by 0.989. Imaginary frequencies are listed in cm^{-1}. [b] Energy relative to W^+ (^6D) + CH_4 reactants including zero point energies (scaled by 0.989). [c] Rotation of methane ligand. [d] Exchange of hydrogens between W and C. [e] Collapses to $HWCH_3^+$ (^2A). [f] Rotation around WC bond. [g] Exchange of methylene hydrogens (CH_2 rock). [h] Rotation of H_2, collapses to ^2A state.

Sextet Surface. Interaction of W^+(^6D, $6s^15d^4$) with methane leads initially to formation of a $W^+(CH_4)$ adduct in which the methane molecule remains intact and largely unperturbed. This potential well is 0.98 eV deep and has the methane binding in an η^2 conformation as a $^6A_1$ state (C_{2v} symmetry), Figure 10.

TABLE 6: Theoretical Structures of [W,C,4H]$^+$ Intermediates and Transition States Calculated at the B3LYP/HW+/6-311++G(3df,3p) Level of Theory[a]

species	state	r(W−H)	r(W−C)	r(C−H)	r(H−H)	∠WCH	∠HCH	∠HWC	∠HWH	∠dihedral
WCH_4^+	$^6A_1$	2.135(2)	2.468	1.087(2), 1.114(2)		59.7(2), 123.3(2)	106.1, 113.4(3), 119.4			±90.0
	^4A	1.933	2.410	1.088, 1.093(2), 1.149		52.2, 83.6, 95.3, 145.1	94.6, 107.0, 109.4, 113.2, 113.8, 116.7			20.4, 115.4, 131.2
	^4A (TS)	1.940	2.409	1.087, 1.092, 1.097, 1.146		76.7, 130.3, 140.6	96.3, 110.4, 118.9, 111.0, 106.0, 112.8	28.0		44.6, −105.7, 143.7
	$^4A_2$ (TS)	2.100(2)	2.421	1.087(2), 1.119(2)		60.0(2), 123.2(2)	105.9(4), 113.5, 120.1			±90.0
	$^4A_1$	2.104(2)	2.428	1.087(2), 1.119(2)		60.0(2), 123.2(2)	105.9(4), 113.7, 120.0			±90.0
	$^4A_2$	2.068(2)	2.374	1.088(2), 1.124(2)		60.6(2), 123.2(2)	105.6(4), 113.5, 121.1			±90.0
	^2A	2.084(2)	2.410	1.087(2), 1.121(2)		59.8(2)	105.8(2), 106.2(2), 113.5, 119.5			20.4, 115.4, 131.2
	$^2A_1$	2.097(2)	2.422	1.087(2), 1.120(2)		59.9(2), 123.3(2)	106.0(4), 113.4, 119.8			±90.0
TS1	$^6A'$	1.694	2.453	1.085(2), 1.087		95.2, 97.6(2)	118.4, 118.7(2)	85.8		±60.1, 180.0
	$^4A'$	1.889, 1.979	2.171	1.090(2), 1.163, 1.188		65.2, 123.7(2)	104.2(2), 105.5(2), 112.4, 125.2	32.1, 33.1		±87.5, 180.0
	^2A	1.903, 1.926	2.146	1.090, 1.091, 1.178, 1.185		62.0, 63.2, 118.6, 129.4	102.7, 102.9, 107.2, 107.9, 112.0, 124.0	33.1, 33.3		−83.4, 95.2, −168.1
$HWCH_3^+$	$^6A'$	1.701	2.418	1.087(3)		96.1(2), 99.5	118.2(2), 119.0	123.6		±60.0, 180.0
	^4A	1.677	2.000	1.090, 1.094, 1.129		88.6, 116.0, 118.5	107.8, 108.1, 113.9	109.9		−23.2, 86.2, −164.2
	^4A (TS)	1.758(2)	1.921	1.093(2), 1.617(2)		58.9(2), 123.0(2)	106.4(4), 114.0, 117.7	51.9(2)		±90.0
	^2A	1.675	1.973	1.089, 1.096, 1,148		82.0, 115.0, 123.0	107.9, 108.1, 114.2	112.5		11.3, −95.1, 158.8
	$^2A''$ (TS)	1.669	2.013	1.095, 1.102(2)		106.0(2), 114.2	107.0, 111.6(2)	108.5		±56.8, 180.0
	$^2A'$	1.677	2.024	1.095 (2), 1.105		103.9, 110.9(2)	109.1(2), 112.6	91.8		±62.9, 180.0
TS2	$^6A'$	1.683, 2.092	2.036	1.091(2), 2.527	2.543	122.0(2)	111.1(2), 115.5	85.0, 169.1	84.1	±86.2
	$^4A'$	1.768, 1.781	1.917	1.093(2), 1.774	0.991	123.0(2)	105.7(2), 113.8	57.2, 89.6	32.4	±88.3
TS3	^4A	1.679, 1.680	2.013	1.092, 1.093	2.757	121.9, 123.8	114.2	100.6, 109.3	110.3	−16.5, 45.2, −132.6, 161.3
	$^2A''$	1.676, 1.894(2)	1.824	1.083, 1.221(2)	2.099	73.9(2), 166.5	111.7(2), 118.5	98.4	67.3	0.0, ±116.6
$(H)_2WCH_2^+$	$^4A''$	1.679(2)	2.012	1.092(2)	2.766	122.8(2)	114.3	106.9(2)	111.0	±29.6, ±148.6
	$^4A'$	1.666(2)	2.036	1.092(2)	1.962	121.4(2)	115.1	113.9(2)	72.2	±41.1, ±121.3
	$^2A'$	1.673(2), 1.944	1.787	1.082, 1.169	2.734	79.2, 165.7	115.1	89.6(2)	109.6	±54.8, ±125.2
	^2A (TS)	1.672, 1.676, 1.944	1.791	1.082, 1.159	2.279, 2.681	79.3, 165.0	115.5	84.1, 95.4	106.5	−3.4, 60.4, −109.4, 166.4
	^2A	1.668, 1.681, 1.903	1.786	1.083, 1.174	2.698	76.9, 168.0	114.8	91.8, 100.7	107.3	−10.6, −71.6, 97.4, −179.6
	$^2A'$ (TS)	1.672(2), 2.505	1.832	1.093, 1.097	2.691	115.3, 128.4	116.4	94.1(2)	107.1	±53.8, ±126.2
	$^2A''$ (TS)	1.673(2), 2.727	2.006	1.091, 1.093	2.670	120.4, 124.8	114.8	98.4(2)	105.8	±53.7, ±126.3
TS4	$^4A''$	1.697(2)	1.950	1.088, 1.099	1.308	115.3, 130.5	114.2	116.2(2)	45.3	±25.4, ±154.6
	^2A	1.822, 1.847	1.824	1.084, 1.124	0.870	95.7, 148.4	115.9	105.5, 119.5	27.4	11.0, 36.7, −147.3, −173.0
$(H_2)WCH_2^+$	$^6A'$	2.118(2)	2.040	1.091(2)	0.777	123.7(2)	112.7	147.3(2)	21.1	±68.3, ±108.1
	$^4A''$	2.029(2)	1.811	1.081, 1.156	0.784	81.8, 162.9	115.3	129.4(2)	22.3	±165.5
	^2A	2.012, 2.049	1.797	1.082, 1.169	0.784	79.8, 165.3	114.9	125.0, 137.2	22.2	−167.2, 167.9, 179.1
	$^2A''$ (TS)	2.038(2)	1.798	1.082, 1.169	0.782	79.8, 165.3	114.8	132.0(2)	22.1	±15.0, ±165.0
TS5	^2A	1.672, 1.757, 1.761	1.753	1.084	1.017	176.3	115.9	56.5, 90.1, 91.5	33.6	52.3, 104.9, 105.5
$(H_2)HWCH^+$	^2A	1.674, 1.824, 1.837	1.744	1.085	0.866	177.0	120.8	67.0, 91.6, 94.4	27.4	−31.4, 75.3, 75.6
	$^2A'$	1.688, 2.473(2)	1.724	1.085	0.756	177.2		89.1, 110.2(2)	17.6	0.0, ±170.6
	$^2A''$ (TS)	1.690, 2.253(2)	1.729	1.085	0.766	176.8		92.0, 105.5(2)	19.6	0.0, ±169.8
$(H_2)HWCH^+$ planar	$^2A'$	1.695, 2.269, 2.302	1.727	1.085	0.768	176.5		88.8, 92.1, 108.1	19.3	0.0, 180.0(2)
	$^2A''$	1.695, 2.172, 2.205	1.733	1.085	0.773	175.9		85.5, 94.8, 105.9	20.3	0.0, 180.0(2)

[a] Bond lengths are in Å. Bond angles are in degrees. Degeneracies are listed in parentheses.

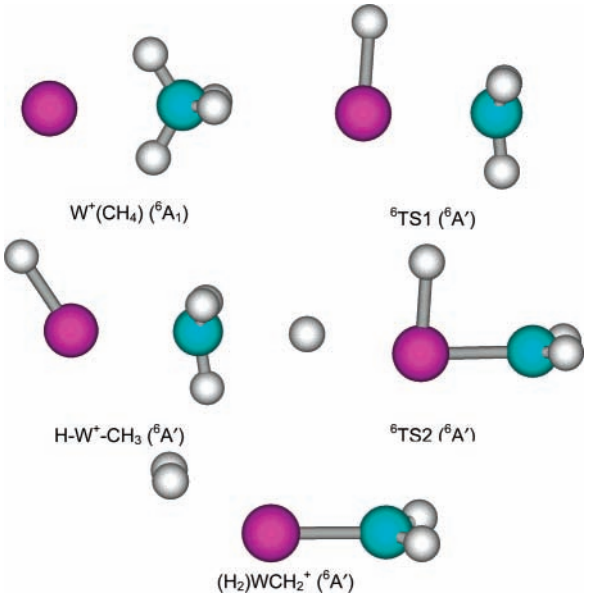

Figure 10. Structures of several intermediates and transition states along the sextet surface of the $[WCH_4]^+$ system calculated at the B3LYP/HW+/6-311++G(3df,3p) level of theory.

Activation of a C−H bond leads to a transition state, ^{6}TS1, leading to the insertion intermediate, H−W^+−CH_3. This ^{6}A′ transition state has C_s symmetry and a HWC bond angle of 86°, Figure 10 and Table 6. Expansion of the HWC bond angle to 123° leads to the $HWCH_3^+$ intermediate, which retains C_s symmetry and the ^{6}A′ state. Other than the HWC bond angle, the intermediate and transition state have similar geometries, consistent with the fact that the transition state energy lies only 0.03 eV higher in energy. In $HWCH_3^+$, the WH bond distance, 1.70 Å, is comparable to that of WH^+ ($^5\Delta$), 1.67 Å, but the WC bond distance of 2.42 Å is substantially longer than in WCH_3^+ (^{5}A), 2.02 Å. This observation along with the WCH bond angles of 96° and 100° (2) indicate that the methyl group is loosely bound to the WH^+ molecule in this state, consistent with the idea that forming a second covalent bond to W^+(^{6}D) would require a quartet state (see below).

Continuing along the sextet surface, the system passes over ^{6}TS2, in which an H_2 bond begins to form. This ^{6}A′ transition state has C_s symmetry, Figure 10, and is quite high in energy, 2.11 eV above the reactants. The W−C bond distance is longer (2.04 Å) than in WCH_2^+(^{4}A″) (1.79 Å), but comparable to WCH_3^+ (^{5}A) (2.02 Å), indicating the CH_2 group forms only a single bond to W^+ as needed to maintain the high spin. Likewise, one of the hydrogens is loosely bound, as indicated by a long W−H bond distance (2.09 Å). Once over this transition state, the system falls into a well corresponding to a $(H_2)WCH_2^+$ intermediate, which has a ^{6}A′ ground state. The H_2 bond distance is 0.78 Å compared to that for free H_2, 0.74 Å, and the geometry of the WCH_2^+ part of the molecule is similar to that for WCH_2^+ ($^6A_1$), Figure 10 and Table 6. This is consistent with the weak H_2−WCH_2^+ bond energy, calculated to be 0.34 eV.

Quartet Surface. Reaction of methane with W^+ in its quartet state also forms a $W^+(CH_4)$ intermediate. The lowest energy state located has the distorted geometry (^{4}A) shown in Figure 11 and lies 0.09 eV below ground state reactants. This is 0.95 eV below the W^+(^{4}F) + CH_4 asymptote, comparable to the W^+-(CH_4) ($^6A_1$) bond energy of 0.98 eV. We also located an η^2 $^4A_1$ state having C_{2v} symmetry and lying only 0.01 eV higher in energy, as well as nearly isoenergetic ^{4}A and η^2 $^4A_2$ (C_{2v} symmetry) states, although these species have imaginary

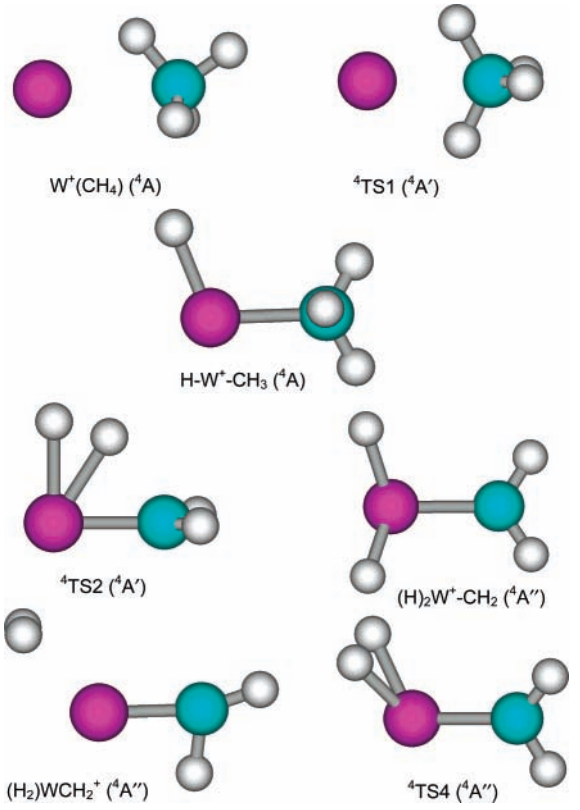

Figure 11. Structures of several intermediates and transition states along the quartet surface of the $[WCH_4]^+$ system calculated at the B3LYP/HW+/6-311++G(3df,3p) level of theory.

frequencies such that they collapse to the $W^+(CH_4)$ (^{4}A) ground state. Including zero point energies, these species actually lie lower in energy than the ^{4}A state, indicating that rotation of the methane ligand is facile. Because of this fluxionality, the transition state for conversion of $W^+(CH_4)$ to the $HWCH_3^+$ intermediate was difficult to locate but involves rotation of the methane ligand to an η^2 geometry (C_s symmetry and near C_{2v}) to allow better interaction between W and C (bond distance of 2.17 Å vs that in $W^+(CH_4)$ of 2.41 Å). Without zero point energy corrections, this ^{4}TS1 (^{4}A′) species was found to lie only 0.07 eV higher than $W^+(CH_4)$ and is 0.034 eV lower in energy after zero point energies are included. Thus, C−H bond activation along the quartet surface is barrierless.

Once over the ^{4}TS1 transition state, the ground state of the insertion intermediate, $HWCH_3^+$ (^{4}A), is formed. This species is the global minimum of the $[W,C,4H]^+$ system, lying 1.39 eV below the ground state asymptote of the reactants (2.25 eV below the quartet reactants). (This agrees with our finding that the $^4B_1$ state of HWH^+ is the global minimum for the analogous $[W,2H]^+$ system.[40]) The W−H and W−C bond distances (1.68 and 2.00 Å) are comparable to those of WH^+ ($^5\Delta$) (1.67 Å) and WCH_3^+ (^{5}A) (2.02 Å), which indicates that both ligands are bound by covalent single bonds. These are formed using sd hybrids on the tungsten cation, leaving three of the π and δ-like nonbonding orbitals on the metal ion singly occupied. This intermediate has a HWC bond angle of 110° and no symmetry because the methyl hydrogen leaning toward the tungsten center, as in WCH_3^+ (^{5}A), prefers to be nearly perpendicular to the WH bond, Figure 11. A transition state for exchanging H atoms between the W and C centers was located 0.86 eV above $HWCH_3^+$ and still 0.42 eV below ^{4}TS1.

From $HWCH_3^+$ (^{4}A), the system can proceed directly to a $(H_2)WCH_2^+$ intermediate via a four-centered transition state ^{4}TS2 having C_s symmetry, Figure 9. In this ^{4}A′ state, Figure

11, the W−H (1.77 and 1.78 Å) bond distances are only slightly longer than those of isolated WH^+ ($^5\Delta$), 1.67 Å, whereas the W−C (1.92 Å) bond distance falls between those of WCH_2^+ ($^4A''$), 1.79 Å, and WCH_3^+ (^5A), 2.02 Å. The ^{4}TS2 transition state lies 0.72 eV above $HWCH_3^+$ (^4A), 0.67 eV below the ground state reactants, and just 0.02 eV above the $(H_2)WCH_2^+$ intermediate. This intermediate has a $^4A''$ ground state, where the WCH_2^+ part of the molecule is very similar in geometry to WCH_2^+ ($^4A''$) and the H_2 bond is essentially fully formed (an H_2 bond length of 0.78 Å compared to that of free H_2, 0.74 Å), Figure 11. This is consistent with the relatively weak interaction, as indicated by the energy required for the $^4A''$ state of $(H_2)WCH_2^+$ to dissociate to WCH_2^+ ($^4A''$) + H_2 ($^1\Sigma_g^+$), 0.52 eV.

Alternatively, $HWCH_3^+$ (^4A) can rearrange by an α-hydrogen migration to form $(H)_2WCH_2^+$ ($^4A''$) by way of ^{4}TS3, Figure 9. This dihydride intermediate, Figure 11, has W−H bond lengths of 1.68 Å, comparable to WH^+ ($^5\Delta$), but an extended W−C bond length, 2.01 Å, compared with WCH_2^+ ($^4A''$), 1.79 Å. This is because once W^+ has formed two covalent WH bonds, it can form only one more covalent bond with carbon and still maintain a quartet spin state (i.e., there is only a single electron in the WC π bond and two nonbonding electrons on W). The ^{4}TS3 transition state lies only 0.005 eV above the $(H)_2WCH_2^+$ ($^4A''$) intermediate, and hence has a very similar geometry, Table 6 (therefore it is not shown in Figure 11). The imaginary frequency corresponds to increasing one of the HWC bond angles while twisting around the WC bond. From $(H)_2WCH_2^+$ ($^4A''$), 1,1-elimination of dihydrogen can occur via ^{4}TS4, which involves the expected motion of the hydrogens after rotation by 90° around the WC bond has occurred. This process again yields the $(H_2)WCH_2^+$ ($^4A''$) intermediate. The ^{4}TS4 transition state lies 0.09 eV above the reactants, which makes this pathway higher in energy than ^{4}TS2 by 0.75 eV.

Doublet Surface. Stable $W^+(CH_4)$ intermediates were also located on the doublet surface. The lowest state nearly has C_{2v} symmetry and lies 0.38 eV above the reactants, 1.36 eV above the $^6A_1$ ground state of $W^+(CH_4)$, and 1.00 eV below the $W^+ + CH_4$ doublet asymptote. A $^2A_1$ state lying 0.20 eV higher in energy was also located. (These complexes exhibit severe spin contamination, $S^2 = 2.6$ instead of 0.75, but this reflects the poorly characterized doublet state of W^+, which has $S^2 = 2.7$.) $^2A_2$, $^2B_1$, and $^2B_2$ states, which lie much higher in energy, all have imaginary frequencies. As for the quartet surface, location of ^{2}TS1 was made difficult because it differed little in energy from $W^+(CH_4)$ (^2A), making the insertion process nearly barrierless once zero point energies were included. With ZPE corrections, ^{2}TS1 lies only 0.03 eV above $W^+(CH_4)$. The geometries of ^{2}TS1 and ^{4}TS1 are very similar, Table 6. (Spin contamination in ^{2}TS1 is reduced from the methane complex but still appreciable, $S^2 = 1.9$.)

The doublet $HWCH_3^+$ species lies 0.50 eV above the comparable species having quartet spin, as would be expected according to Hund's rules for a species forming two covalent bonds and having three nonbonding electrons in nonbonding orbitals. (Because of this, these doublet species are spin contaminated, $S^2 = 1.7$ instead of 0.75.) This doublet intermediate has a structure similar to the quartet spin analogue, Table 6, consistent with coupling of nonbonding electrons. A more symmetric version of this intermediate having C_s symmetry ($^2A''$) is found to be a transition state that collapses to the ^2A ground state, 0.06 eV lower in energy. No four-centered transition state (^{2}TS2) could be found on the doublet surface but formation of ^{2}TS3, Figure 12, involves a barrier of only

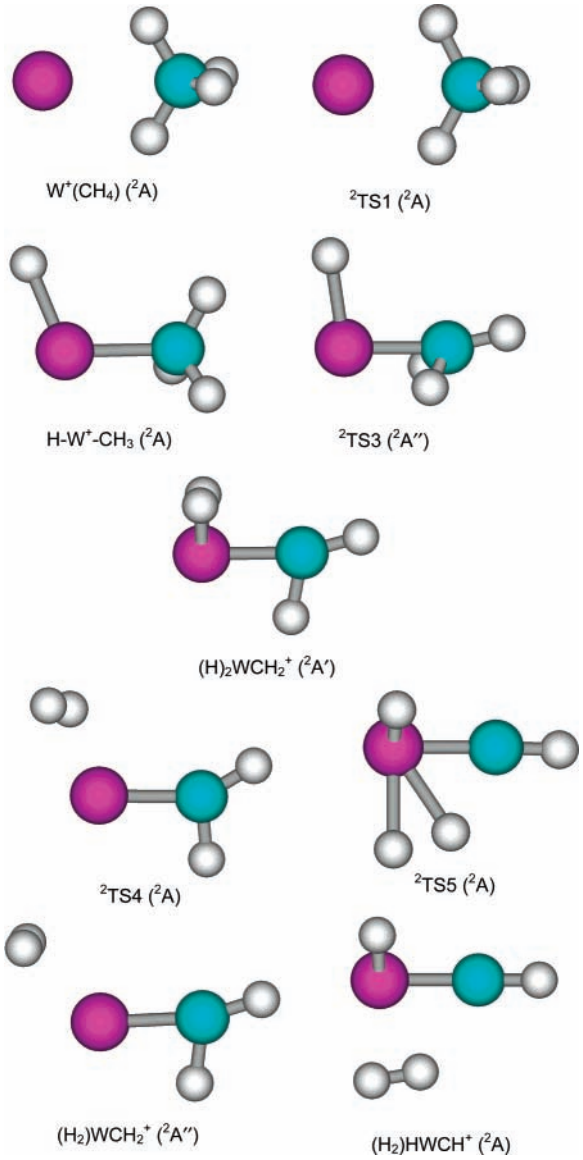

Figure 12. Structures of several intermediates and transition states along the doublet surface of the $[WCH_4]^+$ system calculated at the B3LYP/HW+/6-311++G(3df,3p) level of theory.

0.34 eV. The imaginary frequency corresponds to a very interesting correlated motion in which the two lower hydrogens move from the carbon atom to tungsten and the upper hydrogen atom moves from tungsten back to carbon. A transition state in which only a single hydrogen moved could not be located despite repeated attempts. The ^{2}TS3 transition state leads to the dihydride carbene intermediate, $(H)_2WCH_2^+$, which has a $^2A'$ ground state, Figure 12, and lies only 0.04 eV above the $HWCH_3^+$ (^4A) global minimum species. A doublet spin state for the dihydride carbene is consistent with formation of four covalent bonds to W^+, which leaves one electron in a nonbonding orbital. (Because of this covalency, the doublet dihydride carbene species as well as ^{2}TS3 exhibit no spin contamination, $S^2 = 0.76$.) Note that the two W−H (1.67 Å) and W−C (1.79 Å) bonds are nearly perpendicular to one another, ∠HWC = 89.6°, with bond lengths essentially identical to those of WH^+ ($^5\Delta$) (1.67 Å) and WCH_2^+ ($^4A''$) (1.79 Å).

Because of the interesting hydrogen scrambling reactions 10 and 11, rearrangements of the dihydride carbene were investigated fairly carefully. The lowest energy transformation is rotation about the WC bond, i.e., variation of the HCWH dihedral angle (where the HC bond is bent toward the tungsten).

In the $^2A'$ ground state, this angle is 125°. As this angle is reduced, a barrier of 0.08 eV is found at 60°. Continued rotation leads to a minimum at −11°, i.e., when one of the WH bonds is nearly eclipsed with the HC bond bent toward tungsten. This minimum lies only 0.01 eV above the $^2A'$ ground state and has a geometry ideally situated for elimination of dihydrogen across the WC bond, i.e., 1,2-elimination, although the H−H bond distance is still 1.92 Å for this structure. Further rotation to −54° (total rotation of 180°) leads to a transition state having C_s symmetry ($^2A'$) lying only 0.02 eV above the $^2A'$ ground state. In this rotational motion, the methylene hydrogen bent toward the tungsten is conserved throughout. Exchange of the two methylene hydrogens requires a CH_2 rock motion lying in the plane of symmetry of the $^2A'$ ground state. This has a transition state lying only 0.10 eV above the ground state and leads to the $^2A'$ (54° dihedral angle) transition state.

The doublet dihydride carbene intermediate can lose dihydrogen in a 1,1-elimination process by passing over ^{2}TS4, which lies 1.21 eV higher in energy, but only 0.08 eV above the lowest doublet state of $(H_2)WCH_2^+$ (^2A). The imaginary frequency corresponds to bringing the two hydrogens together, from 2.73 Å in $(H)_2WCH_2^+$ to 0.87 Å in ^{2}TS4 and rotating the H_2 away from the CH_2 group. Thus, the structure of this transition state is similar to the $(H_2)WCH_2^+$ intermediate, but with an elongated and rotated H_2 ligand, Figure 12. This latter intermediate essentially has a plane of symmetry making it a $^2A''$ state, but the computations find that rotation of the H_2 ligand reduces the energy slightly (<0.001 eV), although the symmetric species is the ground state by 0.006 eV once zero point energies are included. The H_2 bond distance is 0.78 Å compared to free H_2 at 0.74 Å. Loss of dihydrogen from $(H_2)WCH_2^+$ to form WCH_2^+ ($^2A''$) + H_2 requires 0.48 eV. (Spin contamination in the $(H_2)WCH_2^+$, $S^2 = 1.6$, and ^{2}TS4, $S^2 = 1.4$, species parallels that for WCH_2^+ ($^2A''$), $S^2 = 1.6$.)

Alternatively, $(H)_2WCH_2^+$ can lose dihydrogen by 1,2-elimination. This involves rotation about the W−C bond (see above) followed by bringing the two H atoms together to form ^{2}TS5 (H−H bond length of 1.02 Å), Figure 12. This yields the $(H_2)HWCH^+$ intermediate in which the dihydrogen, having a bond length of 0.87 Å, is located perpendicular to the plane established by the $HWCH^+$ molecule. Stable geometries in which the complex has C_s symmetry were also located, both with the H_2 molecule in the plane of the $HWCH^+$ molecule ($^2A'$ and $^2A''$ states) and perpendicular to it ($^2A'$ state and a $^2A''$ state that collapses to the ground state). These complexes have much shorter H−H bonds (0.76−0.77 Å) but much longer W−H bonds, >2.17 Å, and lie at higher energies (0.6−0.8 eV), Table 5. Loss of H_2 from the $(H_2)HWCH^+$ intermediate leads directly to formation of $HWCH^+$ ($^2A'$) + H_2 and requires 0.88 eV, consistent with the stronger interaction between W and the H_2 moiety. Overall, the 1,2-elimination pathway is the lower energy pathway for loss of H_2 on the doublet surface, Figure 9. (No spin contamination is found for the various $(H_2)HWCH^+$ species because there is none for $HWCH^+$.)

Discussion

The dehydrogenation reaction of methane by W^+ (^6D) is essentially thermoneutral, as clearly evidenced by the strong isotope dependence, which shifts the reaction from exothermic for CH_4 to endothermic for CD_4. Reasonable agreement between theoretical and experimental bond energies indicates that the dehydrogenation reaction at threshold is either forming WCH_2^+ ($^4A''$) or $HWCH^+$ ($^2A'$). There is strong competition evident between the formation of WCH_2^+ + H_2 and WH^+ + CH_3, implying a common intermediate.

In our previous studies, the activation of methane by atomic metal ions was explained by a simple donor−acceptor model, which leads to an oxidative addition mechanism.[15,24] Such reactions require a metal electronic configurations having an empty acceptor orbital into which the electrons of a bond to be broken are donated. Concomitantly, metal electrons in orbitals having π-symmetry back-donate into the antibonding orbital of the bond to be broken. If the acceptor orbital is occupied, a repulsive interaction can result, leading to inefficient reaction either by more direct abstraction pathways or by introduction of a barrier to the reaction. In this mechanism, oxidative addition of a C−H bond to M^+ forms a $H-M^+-CH_3$ intermediate. Products can be formed by the reductive elimination of H_2 at low energies, by metal−hydrogen or metal−carbon bond cleavage at high energies, and by further dehydrogenation of primary products at still higher energies. For first-row transition metal ions,[15,24] the reductive elimination process proceeds through a four-centered transition state from the $H-M^+-CH_3$ intermediate to a $(H_2)MCH_2^+$ intermediate in which a hydrogen molecule is electrostatically bound to the MCH_2^+ species. This latter intermediate then decomposes by expulsion of H_2. Alternatively, α-H migration to form a dihydride methylene intermediate has been noted for third-row and some second-row metal ions. Reductive elimination of H_2 can then occur from this species, although the present system is the first time 1,2- instead of 1,1-elimination has been suggested. The calculated potential energy surface for the reaction of W^+ with methane, Figure 9, illustrates all of these possible pathways and allows a detailed interpretation of the mechanism for this reaction system.

Mechanism for Dehydrogenation of W^+ with Methane. On the sextet surface, ^{6}TS1 and especially ^{6}TS2 are well above the energy of the ground state $[W,C,2H]^+ + H_2$ product channel, Figure 9. Because W^+ (^6D, $6s^15d^4$) has an occupied valence s orbital, the simple donor−acceptor process is restricted, and because of the high spin, only one covalent bond is formed in the $HWCH_3^+$ ($^6A'$) intermediate, leading to the relatively high energy of this species as well as ^{6}TS1. Because TS2 ideally requires the formation of several covalent bonds to stabilize this transition state, the high-spin sextet state is very high in energy. Thus, reaction of W^+ (^6D) with methane at low energies cannot follow the sextet surface but must involve coupling to the quartet surface where oxidative addition of CH_4 to W^+ produces a ^4A hydridomethyltungsten cation intermediate, $H-W^+-CH_3$, the global minimum on the potential energy surface, Figure 9. The spin−orbit coupling necessary to mix the sextet ground state surface evolving from $W^+(^6D) + CH_4$ with the quartet surface leading to the H_3C-W^+-H intermediate in the entrance channel should be effective for the heavy metal, W^+. On the quartet surface, W^+ (^4F, $6s^15d^4$) can create an empty acceptor and an efficient donor orbital (a doubly occupied $5d\pi$) by coupling with a quartet spin $5d^5$ configuration, essentially an s−d hybridization. This leads naturally to an intermediate in which the W^+ forms two bonds using 6s−5d hybrids.

From $H-W^+-CH_3$ (^4A), the most obvious pathway for producing the $(H_2)WCH_2^+$ ($^4A''$) intermediate is to remain on the quartet surface. As for the first-row transition metal ions, a four-centered transition state, ^{4}TS2, leads directly between these two intermediates with an energy lying below ground state WCH_2^+ ($^4A''$) + H_2 product asymptote, which is formed easily by losing dihydrogen from $(H_2)WCH_2^+$ ($^4A''$). As found for the dehydrogenation reaction of methane with Pt^+ (^2D) and Re^+ (^7S),[13,14] the activation of a second C−H bond (α-H transfer) can lead to formation of dihydridomethylenetungsten cation intermediate, $(H)_2WCH_2^+$ ($^2A'$), but this process involves a spin

change to the doublet. This complex is only 0.04 eV higher in energy than $H-W^+-CH_3$ (^4A). Reductive 1,1-elimination of dihydrogen on the doublet surface passes over ^{2}TS4 and could again couple back to the quartet surface to form the $(H_2)WCH_2^+$ ($^4A''$) intermediate. Alternatively, 1,2-elimination of dihydrogen passes over the lower energy ^{2}TS5 transition state to form $(H_2)HWCH^+$ (^2A), in which the dihydrogen molecule is bound to the $HWCH^+$ geometry. Loss of H_2 easily forms the $HWCH^+$ ($^2A'$) + H_2 products, also calculated to be exothermic from ground state reactants. Overall, the lowest energy pathway appears to be formation of WCH_2^+ ($^4A''$) + H_2 by remaining on the quartet surface, although if interconversion of $H-W^+-CH_3$ (^4A) and $(H)_2WCH_2^+$ ($^2A'$) is facile, then formation of the essentially isoenergetic products, $HWCH^+$ ($^2A'$) + H_2, is probably competitive.

The high-energy feature in the $[W,C,2H]^+$ cross section must correspond to an excited state species lying 0.58 ± 0.18 eV above the ground state. Several species fall into this energy range but the potential energy surface suggests that WCH_2^+ ($^2A''$), $E^* = 0.42$ eV, may account for this feature as formation of this species can occur by rearrangement of the $(H)_2WCH_2^+$ ($^2A'$) intermediate by passing over ^{2}TS4 and then on to products remaining on the doublet surface. Alternatively, formation of WCH_2^+ ($^6A_1$), $E^* = 0.75$ eV, seems plausible but would have to involve a pathway that couples to low-spin surfaces before coupling back to the sextet surface of the products. Such a pathway is not obvious from the present calculations, Figure 9.

Mechanism for Hydrogen Exchange. This potential energy surface also allows an understanding of the hydrogen exchange reactions 10 and 11 observed in the reaction of $[W,C,2H]^+$ with D_2. First, we note that these exchange processes dominate the reaction profile compared to forming $W^+ + CH_2D_2$, reaction 9, even though all three reactions have similar energetics (within 0.1 eV). Ultimately, the fact that the equilibrium assumption for this process yields energetics consistent with the threshold for dehydrogenation measured in the CD_4 system indicates that the relative amounts of dihydrogen vs methane elimination observed in Figure 6 conform to expectations based on the relative free energies of the various species.

If the reaction of WCH_2^+ with D_2 starts and remains on the quartet surface, then the $D-W^+-CH_2D$ (^4A) intermediate is easily formed and can obviously eliminate HD as well as D_2. This explains formation of the $WCHD^+ + HD$ product channel, whereas H_2 loss requires a more complicated process, namely $D-W^+-CH_2D$ (^4A) → $(HD)WCHD^+$ ($^4A''$) → $H-W^+-CHD_2$ (^4A) → $(H_2)WCD_2^+$ ($^4A''$) → WCD_2^+ ($^4A''$) + H_2. The observation of a near equilibrium distribution of these products indicates that these exchanges are facile at low energies. As the available energy increases, however, the need for multiple access to the hydrido methyl intermediate can limit the extent of exchange such that H_2 loss becomes less favored. Indeed, this can explain why the branching ratio between HD and H_2 loss increasingly favors HD loss as the kinetic energy is increased, Figure 6, reflecting the shorter lifetime of the intermediates at these higher energies.

Alternatively, the reaction could start on the doublet $HWCH^+$ ($^2A'$) + D_2 surface, which would readily form the (H)(D)-$WCHD^+$ ($^2A'$) intermediate. In a 1,2-elimination process, this species can lose H_2, HD, or D_2 as observed, but it is not immediately obvious why the branching ratio for HD vs H_2 elimination varies with energy. This may result from the fact that the hydrogens on the methylene moiety of $(H)(D)WCHD^+$ ($^2A'$) are not actually equivalent, as one is bent toward the tungsten atom, Figure 12. At low energies, the lifetime of this intermediate is long enough that the two methylene hydrogens can exchange (by the CH_2 rocking motion found to have a transition state of 0.10 eV, well below ^{2}TS5 at 0.39 eV or the energy needed to eliminate H_2, 1.30 eV), whereas at higher energies, the shorter lifetime means that 1,2-elimination preferentially occurs with the D atom of the CHD ligand (as it is in the correct position for this process having just been added to the carbon), yielding more HD and less H_2. as observed.

Mechanism for Higher Energy Products. As the energy available increases above about 2 eV, W^+-H and W^+-CH_3 products are formed by simple bond cleavages of the $H-W^+-CH_3$ intermediate. These processes, in particular formation of $WH^+ + CH_3$, deplete the population of this intermediate such that the cross section for the dehydrogenation process declines commensurately. Because formation of $WCH_2^+ + H_2$ is thermodynamically preferred by about 2.2 eV (Table 2), this competition indicates that formation of $WH^+ + CH_3$ must be preferred kinetically. This is consistent with a simple bond cleavage of HW^+-CH_3 at elevated kinetic energies, whereas the elimination of H_2 occurs via the more restricted pathway discussed above.

In the reaction of W^+ with CH_4 (CD_4), the WH^+ (WD^+) cross section is dominant at energies above 2.5 eV (Figure 1). This is a typical behavior for the reaction of bare metal ions with hydrogen-containing polyatomic molecules.[15,24,58−60] The observation that the $WH^+ + CH_3$ ($WD^+ + CD_3$) channel dominates the nearly isoenergetic $WCH_3^+ + H$ ($WCD_3^+ + D$) channel, Table 1, is largely a result of angular momentum constraints.[58−62] Briefly, because the $WCH_3^+ + H$ ($WCD_3^+ + D$) channel has a reduced mass of 1.0 (2.0) amu, much smaller than that of the reactants, 14.7 (18.1) amu, it can only be formed by the reactants that come together with smaller orbital angular momenta, i.e., at small impact parameters. In contrast, the $WH^+ + CH_3$ ($WD^+ + CD_3$) channel has a reduced mass of 13.9 (16.4) amu, close to that of the reactants, such that most impact parameters leading to strong interactions between the W^+ and methane can form these products and still conserve angular momentum. We further note that the branching ratio of $\sigma(WD^+)/[\sigma(WCD_3^+) + \sigma(WCD^+)]$ is about 3.7 ± 0.1 around the peak of the WCD^+ cross section (4.5−6.5 eV), consistent with the range of 4−20 suggested as appropriate for a statistical mechanism.[58,63]

At high energies, WC^+ and WCH^+ are formed by dehydrogenation of the primary products, $[W,C,2H]^+$ and WCH_3^+, respectively. The thermochemistry determined above (Table 2) shows that these dehydrogenations require 3.12 ± 0.23 and ~0.89 ± 0.30 eV, respectively. In addition, H atom loss from WCH_3^+, which requires 2.29 ± 0.12 eV, leads to the second feature in the $[W,C,2H]^+$ cross section, Figure 1. This process is observed because the simple bond cleavage is kinetically more favorable at high energies than the more complex dehydrogenation processes. Comparable observations have been made for second-row metal systems[60,62,65,66] and for Pt^+ and Re^+.[13,14]

Conclusions

Ground state W^+ ions are found to be reactive with methane over a wide range of kinetic energies. At low energies, dehydrogenation of CH_4 is slightly exothermic, whereas deuterium substitution makes the reaction with CD_4 slightly endothermic. In both systems, this reaction is efficient and the products react rapidly with additional methane molecules by further dehydrogenation yielding $WC_xH_{2x}^+$ ($WC_xD_{2x}^+$), x = 1−8, in agreement with previous observations at thermal energies.[1,2] At high energies, the dominant process is formation of $WH^+ + CH_3$, which occurs mainly by simple bond cleavage of a $H-W^+-CH_3$ intermediate. This channel is favored over

the $WCH_3^+ + H$ channel because of angular momentum constraints. At higher energies, the $[W,C,2H]^+$ and WCH_3^+ products decompose by dehydrogenation (to form WC^+ and WCH^+, respectively), and at still higher energies, by H atom loss to yield WCH^+ and WCH_2^+.

Analysis of the kinetic energy dependence of the reaction cross sections provides the BDEs of W^+-CH_3, W^+-CH_2, W^+-CH, and W^+-C. Our experimental results for these bond energies are greater than their chromium and molybdenum analogues, Figure 8, a result that can be attributed to enhanced s−d hybridization. Our experimental BDEs are found to be in good agreement with a variety of ab initio calculations from the literature and performed here, Table 2. Whereas the B3LYP functional performs well for multiply bonded species (WC^+, WCH^+, and WCH_2^+), as previously observed by Holthausen et al.,[47] the BHLYP functional is needed to reproduce bond energies for WH^+ and WCH_3^+, as previously concluded by Holthausen et al.[12] Notably the WCH_2^+ species has an alternate geometry, $HWCH^+$, that is comparable in energy, as determined previously by Simon et al.[9] Likewise, we find that WCH_3^+ has low-lying geometries of $HWCH_2^+$ and H_2WCH^+, whereas the HWC^+ geometry lies considerably above the WCH^+ ground state.

Calculations are also used to provide a detailed potential energy surface for the WCH_4^+ system. This potential energy surface shows that the reaction of W^+ (^6D) with methane proceeds via the oxidative addition of one C−H bond to yield a hydridomethyltungsten intermediate, $H-W^+-CH_3$ (^4A), the global minimum. $WH^+ + CH_3$ and $WCH_3^+ + H$ can be formed by simple bond cleavages from this intermediate. At threshold, $[W,C,2H]^+ + H_2$ formation can occur by two possible pathways: (a) rearrangement through the four-centered $^4TS2$ transition state to form WCH_2^+ ($^4A''$) + H_2 or (b) α-H migration to form the dihydridomethylene tungsten cation, $(H)_2WCH_2^+$ ($^2A'$), followed by reductive 1,2-elimination of dihydrogen to yield $HWCH^+$ ($^2A'$) + H_2. Formation of an excited state of this product is also observed and is most plausibly attributed to formation of WCH_2^+ ($^2A''$) + H_2. Overall, dehydrogenation of methane by W^+ requires at least one spin change and possibly two along the lowest energy path available.

Acknowledgment. This work is supported by the National Science Foundation, Grant No. CHE-0451477. Thanks to Karl Irikura and Philippe Maitre for their comments on the manuscript.

References and Notes

(1) Irikura, K. K.; Beauchamp, J. L. *J. Am. Chem. Soc.* **1991**, *113*, 2769.
(2) Irikura, K. K.; Beauchamp, J. L. *J. Phys. Chem.* **1991**, *95*, 8344.
(3) Mourgues, P.; Ferhati, A.; McMahon, T. B.; Ohanessian, G. *Organometallics* **1997**, *16*, 210.
(4) Ferhati, A.; McMahon, T. B.; Ohanessian, G. *Soc. Chim. Fr.* **1993**, *130*, 3.
(5) Ferhati, A.; McMahon, T. B.; Ohanessian, G. *J. Am. Chem. Soc.* **1996**, *118*, 5997.
(6) Beckner, S. W.; MacMahon, T. J.; Byrd, G. D.; Freiser, B. S. *Inorg. Chem.* **1989**, *28*, 3511.
(7) Ranasinghe, Y. A.; MacMahon, T. J.; Freiser, B. S. *J. Phys. Chem.* **1991**, *95*, 7721.
(8) Jones, W. D. *Acc. Chem. Res.* **2003**, *36*, 140.
(9) Simon, A.; Lemaire, J.; Boissel, P.; Maitre, P. *J. Chem. Phys.* **2001**, *115*, 2510.
(10) Irikura, K. K.; Goddard, W. A., III. *J. Am. Chem. Soc.* **1994**, *116*, 8733.
(11) Ohanessian, G.; Goddard, W. A., III. *Acc. Chem. Res.* **1990**, *23*, 386.
(12) Holthausen, M. C.; Heinemann, C.; Cornehl, H. H.; Koch, W.; Schwarz, H. *J. Chem. Phys.* **1995**, *102*, 4931.
(13) Zhang, X.-G.; Liyanage, R.; Armentrout, P. B. *J. Am. Chem. Soc.* **2001**, *123*, 5563.
(14) Armentrout, M. M.; Li, F.-X.; Armentrout, P. B. *J. Phys. Chem. A*, **2004**, *108*, 9660.
(15) Armentrout, P. B. In *Selective Hydrocarbon Activation: Principles and Progress*; Davies, J. A., Watson, P. L., Greenberg, A., Liebman, J. F., Eds.; VCH: New York, 1990; pp 467−533.
(16) Armentrout, P. B. In *Gas-Phase Inorganic Chemistry*; Russell D. H., Ed.; Plenum: New York, 1989. Armentrout, P. B.; Beauchamp, J. L. *Acc. Chem. Res.* **1989**, *22*, 315.
(17) Armentrout, P. B. *Science* **1991**, *25*, 1175.
(18) Armentrout, P. B. *Annu. Rev. Phys. Chem.* **1990**, *41*, 313.
(19) van Koppen, P. A. M.; Kemper, P. R.; Bowers, M. T. *J. Am. Chem. Soc.* **1992**, *114*, 1083.
(20) van Koppen, P. A. M.; Kemper, P. R.; Bowers, M. T. In *Organometallic Ion Chemistry*; Freiser, B. S., Ed.; Kluwer: Dordrecht, The Netherlands, 1995; pp 157−196.
(21) Allison, J. *Prog. Inorg. Chem.* **1986**, *34*, 627.
(22) Squires, R. R. *Chem. Rev.* **1987**, *87*, 623.
(23) *Gas-Phase Inorganic Chemistry*; Russell, D. H., Ed.; Plenum: New York, 1989. Eller, K.; Schwarz, H. *Chem. Rev.* **1991**, *91*, 1121.
(24) Armentrout, P. B. In *Organometallic Bonding and Reactivity*; Brown, J. M.; Hofmann, P., Eds.; Topics in Organometallic Chemistry, Vol. 4; Springer-Verlag: Berlin, 1999; pp 1−45.
(25) Armentrout, P. B.; Georgiadis, R. *Polyhedron* **1988**, *7*, 1573.
(26) Armentrout, P. B.; Clemmer, D. E. In *Energetics of Organometallic Species*; Simoes, J. A. M., Beauchamp, J. L., Eds.; Kluwer: Dordrecht, The Netherlands, 1992; p 321.
(27) Armentrout, P. B.; Kickel, B. L. *Organometallic Ion Chemistry*; Freiser B. S., Ed.; Kluwer: Dordrecht, The Netherlands, 1995; p 1.
(28) Haynes, C. L.; Chen, Y.-M.; Armentrout, P. B. *J. Phys. Chem.* **1995**, *99*, 9110.
(29) Haynes, C. L.; Chen, Y.-M.; Armentrout, P. B. *J. Phys. Chem.* **1996**, *100*, 111.
(30) Loh, S. K.; Hales, D. A.; Lian, L.; Armentrout, P. B. *J. Chem. Phys.* **1989**, *90*, 5466.
(31) Schultz, R. H.; Armentrout, P. B. *Int. J. Mass Spectrom. Ion. Processes* **1991**, *107*, 29.
(32) Gerlich, D. *Adv. Chem. Phys.* **1992**, *82*, 1.
(33) Ervin, K. M.; Armentrout, P. B. *J. Chem. Phys.* **1985**, *83*, 166.
(34) Haynes, C. L.; Armentrout, P. B. *Organometallics* **1994**, *13*, 3480.
(35) Sievers, M. R.; Chen, Y.-M.; Elkind, J. L.; Armentrout, P. B. *J. Phys. Chem.* **1996**, *100*, 54.
(36) Kickel, B. L.; Armentrout, P. B. *J. Am. Chem. Soc.* **1995**, *117*, 4057.
(37) Kickel, B. L.; Armentrout, P. B. *J. Am. Chem. Soc.* **1995**, *117*, 764.
(38) Clemmer, D. E.; Chen, Y.-M.; Khan, F. A.; Armentrout, P. B. *J. Phys. Chem.* **1994**, *98*, 6522.
(39) Moore, C. E. *Atomic Energy Levels*, NSRDS−NBS, 1971, 35/Vol. III.
(40) Zhang, X.-G.; Rue, C.; Shin, S.-Y.; Armentrout, P. B. *J. Chem. Phys.* **2002**, *116*, 5574.
(41) Becke, A. D. *J. Chem. Phys.* **1993**, *98*, 5648.
(42) Lee, C.; Yang, W.; Parr, R. G. *Phys. Rev. B* **1988**, *37*, 785.
(43) Frisch, M. J.; Trucks, G. W.; Schlegel, H. B.; Scuseria, G. E.; Robb, M. A.; Cheeseman, J. R.; Zakrzewski, V. G.; Montgomery, J. A., Jr.; Stratmann, R. E.; Burant, J. C.; Dapprich, S.; Millam, J. M.; Daniels, A. D.; Kudin, K. N.; Strain, M. C.; Farkas, O.; Tomasi, J.; Barone, V.; Cossi, M.; Cammi, R.; Mennucci, B.; Pomelli, C.; Adamo, C.; Clifford, S.; Ochterski, J.; Petersson, G. A.; Ayala, P. Y.; Cui, Q.; Morokuma, K.; Malick, D. K.; Rabuck, A. D.; Raghavachari, K.; Foresman, J. B.; Cioslowski, J.; Ortiz, J. V.; Stefanov, B. B.; Liu, G.; Liashenko, A.; Piskorz, P.; Komaromi, I.; Gomperts, R.; Martin, R. L.; Fox, D. J.; Keith, T.; Al-Laham, M. A.; Peng, C. Y.; Nanayakkara, A.; Gonzalez, C.; Challacombe, M.; Gill, P. M. W.; Johnson, B. G.; Chen, W.; Wong, M. W.; Andres, J. L.; Head-Gordon, M.; Replogle, E. S.; Pople, J. A. *Gaussian 98*, revision A.7; Gaussian, Inc.: Pittsburgh, PA, 1998.
(44) Hay, P. J.; Wadt, W. R. *J. Chem. Phys.* **1985**, *82*, 299.
(45) Ohanessian, G.; Brusich, M. J.; Goddard, W. A., III. *J. Am. Chem. Soc.* **1990**, *112*, 7179.
(46) Foresman, J. B.; Frisch, Æ. *Exploring Chemistry with Electronic Structure Methods*, 2nd Ed.; Gaussian: Pittsburgh, PA, 1996.
(47) Holthausen, M. C.; Mohr, M.; Koch, W. *Chem. Phys. Lett.* **1995**, *240*, 245.
(48) Perdew, J. P. *Phys. Rev.* **1986**, *33*, 8822.
(49) Adamo, C.; Barone, V. *J. Chem. Phys.* **1998**, *108*, 664.
(50) Gioumousis, G.; Stevenson, D. P. *J. Chem. Phys.* **1958**, *29*, 292.
(51) Chase, M. W. *NIST-JANAF Thermochemical Tables*, 4th ed.; Journal of Physical and Chemical Reference Data, Monograph 9; AIP: Melville, NY, 1998; p 1.

(52) Elkind, J. L.; Armentrout, P. B. *J. Phys. Chem.* **1987**, *86*, 1868.
(53) Fisher, E. R.; Armentrout, P. B. *J. Am. Chem. Soc.* **1992**, *114*, 2039.
(54) Georgiadis, R.; Armentrout, P. B. *Int. J. Mass Spectrom. Ion Processes* **1989**, *89*, 227.
(55) Georgiadis, R.; Armentrout, P. B. *J. Phys. Chem.* **1988**, *92*, 7067.
(56) Peng, C.; Schlegel, H. B. *Isr. J. Chem.* **1994**, *33*, 449.
(57) Peng, C.; Ayala, P. Y.; Schlegel, H. B.; Frisch, M. J. *J. Comput. Chem.* **1996**, *17*, 49.
(58) Sunderlin, L. S.; Armentrout, P. B. *J. Am. Chem. Soc.* **1989**, *111*, 3845.
(59) Aristov. N.; Armentrout, P. B. *J. Phys. Chem.* **1987**, *91*, 6178.
(60) Chen, Y.-M.; Sievers, M. R.; Armentrout, P. B. *Int. J. Mass Spectrom. Ion Processes* **1997**, *167/168*, 195.
(61) Sunderlin, L. S.; Armentrout, P. B. *J. Phys. Chem.* **1988**, *92*, 1209.
(62) Chen, Y.-M.; Armentrout, P. B. *J. Phys. Chem.* **1995**, *99*, 10775.
(63) Aristov, N.; Armentrout, P. B. *J. Am. Chem. Soc.* **1986**, *108*, 1806.
(64) Chen, Y.-M.; Armentrout, P. B. *J. Am. Chem. Soc.* **1995**, *117*, 9291.
(65) Armentrout, P. B.; Chen, Y.-M. *J. Am. Soc. Mass Spectrom.* **1999**, *10*, 821.
(66) Sievers, M. R.; Chen, Y.-M.; Haynes, C. L.; Armentrout, P. B. *Int. J. Mass Spectrom. Ion Processes* **2000**, *195/196*, 149.